A&A 665, A156 (2022)
https://doi.org/10.1051/0004-6361/202244164

Astronomy & Astrophysics

Is ozone a reliable proxy for molecular oxygen?

I. The O_2–O_3 relationship for Earth-like atmospheres

Thea Kozakis, João M. Mendonça, and Lars A. Buchhave

National Space Institute, Technical University of Denmark, Elektrovej, 2800 Kgs. Lyngby, Denmark
e-mail: theakozakis@space.dtu.dk

Received 1 June 2022 / Accepted 7 August 2022

ABSTRACT

Molecular oxygen (O_2) paired with a reducing gas is regarded as a promising biosignature pair for the atmospheric characterization of terrestrial exoplanets. In circumstances when O_2 may not be detectable in a planetary atmosphere (e.g., at mid-IR wavelengths) it has been suggested that ozone (O_3), the photochemical product of O_2, could be used as a proxy to infer the presence of O_2. However, O_3 production has a nonlinear dependence on O_2 and is strongly influenced by the UV spectrum of the host star. To evaluate the reliability of O_3 as a proxy for O_2, we used `Atmos`, a 1D coupled climate and photochemistry code, to study the O_2–O_3 relationship for "Earth-like" habitable zone planets around a variety of stellar hosts (G0V-M5V) and O_2 abundances. Overall, we found that the O_2–O_3 relationship differed significantly with stellar hosts and resulted in different trends for hotter stars (G0V-K2V) versus cooler stars (K5V-M5V). Planets orbiting hotter host stars counter-intuitively experience an increase in O_3 when O_2 levels are initially decreased from 100% Earth's present atmospheric level (PAL), with a maximum O_3 abundance occurring at 25–55% PAL O_2. As O_2 abundance initially decreases, larger amounts of UV photons capable of O_2 photolysis reach the lower (denser) regions of the atmosphere where O_3 production is more efficient, thus resulting in these increased O_3 levels. This effect does not occur for cooler host stars (K5V-M5V), since the weaker incident UV flux does not allow O_3 formation to occur at dense enough regions of the atmosphere where the faster O_3 production can outweigh a smaller source of O_2 from which to create O_3. Thus, planets experiencing higher amounts of incident UV possessed larger stratospheric temperature inversions, leading to shallower O_3 features in planetary emission spectra. Overall it will be extremely difficult (or impossible) to infer precise O_2 levels from an O_3 measurement, however, with information about the UV spectrum of the host star and context clues, O_3 will provide valuable information about potential surface habitability of an exoplanet.

Key words. astrobiology – planets and satellites: terrestrial planets – planets and satellites: atmospheres

1. Introduction

In the search for life in the Universe, molecular oxygen (O_2) is commonly recognized as a promising atmospheric biosignature gas. However, while O_2 is largely created by biological sources on Earth, it can also be produced abiotically in a variety of settings, and thus alone would not constitute a guarantee of life (e.g., Hu et al. 2012; Wordsworth & Pierrehumbert 2014; Domagal-Goldman et al. 2014; Tian et al. 2014; Luger & Barnes 2015; Gao et al. 2015; Harman et al. 2015). Instead of being a standalone biosignature, O_2 as a biosignature will be most powerful when detected simultaneously with a reducing gas as a "disequilibrium biosignature pair" (e.g., Lovelock 1965; Lederberg 1965; Lippincott et al. 1967), and when evidence of abiotic O_2 production scenarios can be ruled out (see Meadows 2017; Meadows et al. 2018b for a review).

In scenarios where O_2 is not directly detectable, it has been suggested that its photochemical product ozone (O_3) could be used as a proxy for O_2 (e.g., Leger et al. 1993; Des Marais et al. 2002; Segura et al. 2003; Léger et al. 2011; Meadows et al. 2018b). Using O_3 as a proxy for O_2 would be extremely useful in two particular scenarios: 1) at wavelengths where O_2 features are not present (i.e., mid-infrared wavelengths), and 2) when O_2 is present in small amounts (as it was for a significant fraction of Earth's geological history).

The mid-infrared wavelength region (MIR; 3–20 μm) provides an excellent opportunity for the search for life, as it contains features for multiple biosignature gases, as well for gaseous species that could provide evidence for or against biological O_2 production (Des Marais et al. 2002; Schwieterman et al. 2018; Quanz et al. 2021). Furthermore, thermal emission observations are less impacted by clouds (e.g., Kitzmann et al. 2011), and could also allow measurements of a planet's surface temperature (Des Marais et al. 2002). The collisionally-induced absorption O_2 feature at 6.4 μm is the only MIR feature that allows for the direct detection of O_2, although it would be extremely difficult to use for abundances of O_2 consistent with biological production (Fauchez et al. 2020). It will, however, be useful for identifying high-O_2 desiccated atmospheres, a possible mechanism for abiotic O_2 production (Luger & Barnes 2015; Tian 2015). Inferring the presence of biologically produced O_2 will be restricted to indirect detections via the 9.7 μm O_3 feature in the MIR.

In addition, although O_2 has existed in appreciable amounts on Earth for a significant part of its history, it has only existed in large amounts for a relatively short period of time, posing a fundamental drawback to O_2 as a biosignature (Meadows et al. 2018b). Molecular oxygen was first created produced biologically ~2.7 Ga (billion years ago) by oxygenic photosynthesis via cyanobacteria, although it did not build up to appreciable amounts in Earth's atmosphere until the Great Oxidation Event (GOE) ~2.45 Ga (see e.g., Catling & Kasting 2017 for a review). Although the Phanerozoic era (541 Ma–present day) saw the widespread colonization of land plants and O_2 levels comparable

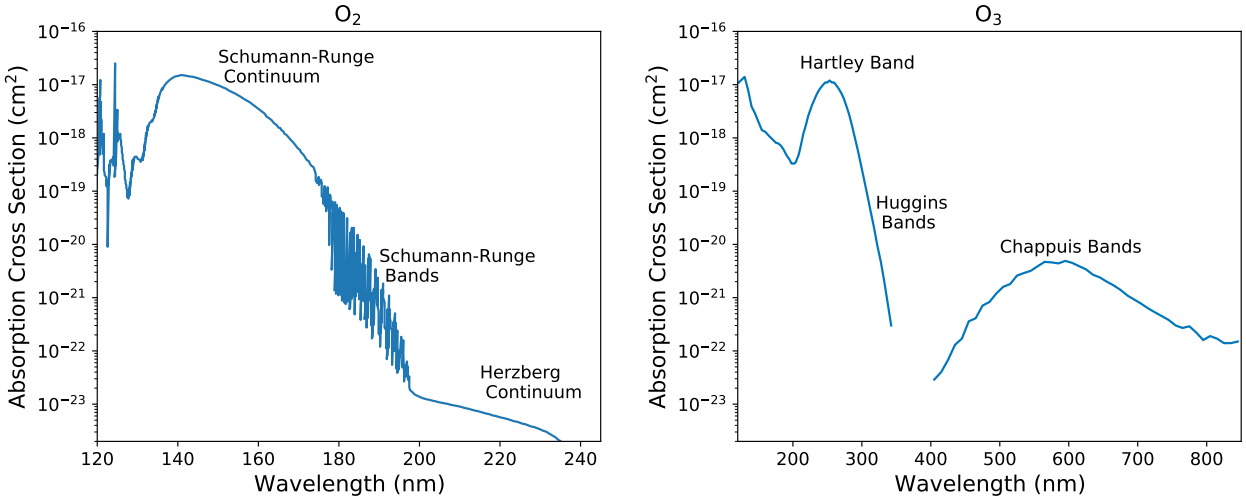

Fig. 1. Absorption cross sections of O_2 (*left*) and O_3 (*right*), both plotted on the same y-axis scale to enable easier comparison. The *y*-axis is the same for both to enable easier comparison. Relevant O_2 bands are the Schumann–Runge continuum (137–175 nm), the Schuman–Runge bands (175–200 nm), and the Herzberg continuum (195–242 nm). For less than 175 nm an excited O atom, the O(^{1}D) radical, is formed along with a ground state O atom during photolysis. O_3 bands are the Hartley bands (200–300 nm), the Huggins bands (310–350 nm), and the Chappuis bands (410–750 nm). Photolysis within the Hartley bands will produce the O(^{1}D) radical while other O_3 bands create a ground state O atom. Absorption cross section data is from Brasseur & Solomon (2005).

to our present atmospheric level (PAL), during the Proterozoic era (2.5 Ga–541 Ma) it is expected O_2 levels could have been significantly lower (Catling & Kasting 2017; Lenton & Daines 2017; Dahl & Arens 2020). As a result, it is likely that O_2 only would have been detectable on Earth for the last ∼0.5 Gyr. However, since O_3 is a logarithmic tracer of O_2, it is possible that O_3 could be capable of revealing small, undetectable amounts of O_2 (e.g., Kasting et al. 1985; Leger et al. 1993; Des Marais et al. 2002; Segura et al. 2003; Léger et al. 2011). Additionally, a detection of O_3 could provide information about UV shielding, and whether surface life is adequately protected from high-energy UV capable of DNA damage.

Some studies have suggested or already adopted O_3 as a substitute for O_2 (e.g., Segura et al. 2003, Kaltenegger et al. 2020, Lin et al. 2021), and others have noted a potentially powerful "triple biosignature" in planetary emission with CO_2, H_2O, and O_3, where O_2 spectral features are absent (Selsis et al. 2002). O_3 is also expected to build up in the stratospheres of planets, allowing characterization via transmission spectroscopy (e.g., Bétrémieux & Kaltenegger 2013, 2014; Misra et al. 2014; Meadows et al. 2018b).

However, it is uncertain how reliably a measurement of O_3 could allow us to infer the amount of O_2. Ozone is known to have a nonlinear relationship with O_2, as well as a strong dependence on the UV spectrum of the host star (Ratner & Walker 1972; Kasting & Donahue 1980; Kasting et al. 1985; Segura et al. 2003; Rugheimer et al. 2013). Although several studies have modeled the O_2–O_3 relationship for varying O_2 abundances and different stellar hosts (e.g., Ratner & Walker 1972; Levine et al. 1979; Kasting & Donahue 1980; Kasting et al. 1985; Segura et al. 2003; Gregory et al. 2021), there has been no in-depth study evaluating the ability of O_3 to predict O_2 as a biosignature. In this series of papers, we will explore the O_2–O_3 relationship in depth for a variety of stellar hosts and atmospheric conditions. For this first paper, we focus on the O_2–O_3 relationship for "Earth-like" planets for different stellar hosts. Here, we take Earth-like to mean a planet that has the same composition and size as Earth, receives the equivalent total incident flux from the Sun as modern Earth, and has a similar atmospheric composition. This study currently contains the largest number of models run with a fully coupled climate and photochemistry code dedicated to understanding the O_2–O_3 relationship, along with exploring the widest range of stellar hosts as well as the largest number of different O_2 atmospheric abundances.

2. Chemistry of O_3 production and destruction

In this section, we give a brief overview of the most important reactions for the production and destruction of O_3. The wavelength-dependent absorption cross sections for O_2 and O_3 are shown in Fig. 1 as a reference for the reader, as they determine photolysis rates in different wavelength regions. Incident stellar UV flux as well as the amount of nitrogen- and hydrogen-bearing species primarily control the concentration of O_3 in the atmosphere.

2.1. The Chapman mechanism

Ozone is primarily created in the stratosphere by a set of reactions called the Chapman mechanism (Chapman 1930). These reactions begin with the photolysis of O_2,

$$O_2 + h\nu \rightarrow O + O \ (175 < \lambda < 242 \text{ nm}), \quad (1)$$

which creates ground state O atoms (also written as O(^{3}P)), which are highly reactive due to two unpaired electrons. These O atoms then combine with O_2 molecules to form O_3,

$$O + O_2 + M \rightarrow O_3 + M, \quad (2)$$

where M is a background molecule that carries away excess energy. Reaction (2) is a 3-body reaction, meaning it is more efficient at lower temperatures and higher atmospheric densities. It is faster in denser atmospheric regions with a larger availability of O atoms, causing bulk of O_3 on Earth to exist in the stratosphere rather than at higher altitudes.

Photolysis of O_2 can also occur higher in the atmosphere with higher energy photons,

$$O_2 + h\nu \rightarrow O \ + O(^1D) \ (\lambda < 175 \text{ nm}), \quad (3)$$

where the $O(^1D)$ radical is created along with a ground state O atom. Free radicals are by nature extremely reactive as they have at least one unpaired valence electron. Thus, they tend to have extremely brief lifetimes. The $O(^1D)$ radical can return to the ground state by being "quenched" via a collision with a background molecule,

$$O(^1D) + M \rightarrow O + M, \quad (4)$$

or it can react with another molecule. Reactions with other molecules will be further explored in Sects. 2.2 and 4.1.

Although O_2 absorption cross sections are significantly larger at wavelengths that produce $O(^1D)$ radicals (<175 nm; see Fig. 1), these photons are absorbed high in the atmosphere and therefore do not contribute to the creation of stratospheric O_3 on modern Earth. Absorption caused by Lyman-α photons (121.6 nm) is generally absorbed in the mesosphere, and photons in the Schumann–Runge continuum (130–175 nm) are absorbed in the thermosphere. Also note that some wavelengths shorter than Lyman-α can ionize O_2, although that wavelength region is not included in our photochemistry model due to the low amount of photons in that region emitted by GKM stars (see Sect. 3.1).

Although O_2 photolysis from these higher energy photons (<175 nm) occurs above the stratosphere on modern Earth, planets with different amounts of atmospheric O_2 would experience absorption of these photons at varying atmospheric altitudes. Less O_2 would allow high energy photons to travel deeper into the atmosphere before absorption via O_2 photolysis. Although this will not cause the bulk of O_3 formation, it will impact the upper atmospheric chemistry by creating more $O(^1D)$ at lower altitudes. The effects of this will discussed at length in Sect. 4.1.

Once O_3 is created by Reaction (2), it is often quickly photolyzed. O_3 photolysis from a photon in the Hartley band (200–300 nm) will create an $O(^1D)$ radical, while photons from the lower energy Huggins bands (310–350 nm), Chappuis bands (410–750 nm), and longer wavelengths will create a ground state O atom,

$$O_3 + h\nu \rightarrow O_2 + O(^1D) (\lambda < 310 \text{ nm}), \quad (5)$$

$$O_3 + h\nu \rightarrow O_2 + O \ (310 < \lambda < 1140 \text{ nm}). \quad (6)$$

Photons with wavelengths shorter than 200 nm are often absorbed high in the atmosphere by O_2 and other molecules. As with O_2 photolysis, $O(^1D)$ radicals created by Reaction (5) will either be quenched by a background molecule and returned to the ground state (Reaction (4)), or they will react with other molecules.

Photolysis of O_3 is not seen as a loss of O_3, as the resulting O atom and O_2 molecule often quickly recombine into O_3 via Reaction (2). Due to the rapid cycling between O_3 and O, it is instead the conversion of O_3 + O (called "odd oxygen") into O_2 that actually results in a loss of O_3, as occurs in the final reaction of the Chapman mechanism,

$$O_3 + O \rightarrow 2O_2. \quad (7)$$

Odd oxygen (O_3 + O) being converted into O_2 is considered a loss of O_3 because the photolysis of O_2 (Reactions (1), (3)) is the slowest of the Chapman mechanism reactions, and the limiting factor in O_3 production. Therefore the loss of odd oxygen on long timescales causes a true decrease in O_3.

2.2. Catalytic cycles of HO_x and NO_x

The Chapman mechanism on its own overestimates the amount of atmospheric O_3 because it does not take into account catalytic cycles that destroy O_3. These destruction cycles follow the format,

$$\begin{aligned} X + O_3 &\rightarrow XO + O_2 \\ XO + O &\rightarrow X + O_2 \\ \hline \text{Net:} \quad O_3 + O &\rightarrow 2O_2 \end{aligned}$$

where X is a free radical. During this process X and XO will cycle between each other while converting odd oxygen (O_3 + O) into O_2, similarly to the last step of the Chapman mechanism (Reaction (7)). As stated above, this results in the overall loss of O_3 because O_2 photolysis is the limiting reaction of O_3 formation. X and XO can cycle between each other and continuously destroy O_3 until reactions that convert either X or XO into non-reactive "reservoir" species occur. The primary catalytic cycles of O_3 destruction in modern Earth's atmosphere are the HO_x (hydrogen oxide) and NO_x (nitrogen oxide) catalytic cycles. We note that on modern Earth there are also O_3 destroying catalytic cycles that are powered by molecular compounds primarily created anthropogenically (e.g., chlorine and bromine cycles; Crutzen & Lelieveld 2001), but they will not be included in this study.

The HO_x catalytic cycle is powered by the OH (hydroxyl) and HO_2 (hydroperoxyl) radicals. When an $O(^1D)$ radical is created either by photolysis of O_2 (Reaction (3)) or O_3 (Reaction (5)) it can react with H_2O to form OH,

$$H_2O + O(^1D) \rightarrow OH + OH. \quad (8)$$

The OH radical is a major sink for multiple atmospheric gases (e.g., CH_4, CO) and is often called the 'detergent of the atmosphere' for this reason. It destroys O_3 during the HO_x catalytic cycle as follows,

$$OH + O_3 \rightarrow HO_2 + O_2, \quad (9)$$

$$HO_2 + O \rightarrow OH + O_2. \quad (10)$$

In addition to this primary destruction cycle, other HO_x cycles can contribute significantly to O_3 destruction via,

$$OH + O_3 \rightarrow HO_2 + O_2, \quad (9)$$

$$HO_2 + O_3 \rightarrow OH + 2O_2, \quad (11)$$

resulting in two O_3 molecules converted to three O_2 molecules, or,

$$OH + O \rightarrow H + O_2, \quad (12)$$

$$H + O_2 + M \rightarrow HO_2 + M, \quad (13)$$

$$HO_2 + O \rightarrow OH + O_2, \quad (10)$$

with a net result of two O atoms converted into an O_2 molecule. Because OH production via $O(^1D)$ is a byproduct of the Chapman mechanism, HO_x catalytic cycle efficiency can be increased with higher rates of O_3 formation. This process can be slowed through reactions that convert OH/HO_2 into a reservoir species such as H_2O, HNO_2, or H_2O_2, which are significantly less reactive.

The NO_x catalytic cycle destroys O_3 with the NO (nitric oxide) and NO_2 (nitrogen dioxide) radicals. The primary source of these radicals in the stratosphere is from N_2O (nitrous oxide) which is biologically produced by nitrification and denitrification processes within soil. N_2O can additionally be produced anthropogenically, primarily through agriculture. It is converted into NO by interactions with the $O(^1D)$ radical,

$$N_2O + O(^1D) \rightarrow NO + NO. \quad (14)$$

A secondary source of NO is production via lightning in the upper troposphere, which can then be transported into the lower stratosphere. The NO_x catalytic cycle destroys O_3 as follows:

$$NO + O_3 \rightarrow NO_2 + O_2, \quad (15)$$

$$NO_2 + O \rightarrow NO + O_2. \quad (16)$$

NO_x can destroy O_3 with the following cycle as well,

$$NO + O_3 \rightarrow NO_2 + O_2, \quad (15)$$

$$NO_2 + O_3 \rightarrow NO_3 + O_2. \quad (17)$$

$$NO_3 + h\nu \rightarrow NO + O_2. \quad (18)$$

with a net conversion of two O_3 molecules into three O_2 molecules. NO_x reactions are highly temperature dependent and are faster at hotter temperatures. The main reservoir species associated with NO_x are HNO_3 and N_2O_5, which have slow photolysis rates.

We note that although in the stratosphere NO_x destroys O_3 through this catalytic cycle, that lower in the atmosphere it can help create O_3 through the "smog mechanism" (see Sect. 5.2). This low altitude O_3 is a pollutant that can cause biological damage. In this study we will focus on the majority of O_3 in the stratosphere created by the Chapman mechanism. In this study we will focus on the efficiency of the Chapman mechanism, along with the ability of the HO_x and NO_x catalytic cycles to destroy O_3 for varying O_2 levels around different host stars.

3. Methods

3.1. Atmospheric models

We modeled planetary atmospheres with `Atmos`[1], a 1D coupled climate and photochemistry code to explore O_3 formation for varying levels of O_2 on Earth-like planets around a variety of host stars. Numerous studies have used either of these climate or photochemistry modules, as well as both coupled (e.g., Arney et al. 2017; Meadows et al. 2018a; Lincowski et al. 2018; Madden & Kaltenegger 2020; Gregory et al. 2021; Teal et al. 2022). We give a brief overview of `Atmos` and refer readers to Arney et al. (2016) and Meadows et al. (2018a) for extensive details.

The photochemistry model originates from Kasting (1979) and was expanded upon and updated by Zahnle et al. (2006). It has been used extensively by many studies (e.g., Kasting & Donahue 1980; Segura et al. 2003, 2005, 2010; Domagal-Goldman et al. 2014; Gregory et al. 2021). The atmosphere is broken up in 200 plane parallel layers from 0 to 100 km. The abundance of each gaseous species is calculated simultaneously with the flux and continuity equations using a reverse-Euler method for individual atmospheric layers. Vertical transport between different layers include molecular and eddy diffusion. Radiative transfer is computed with a δ-2-stream method as described in Toon et al. (1989). For modern Earth `Atmos` uses 50 gaseous species, with nine of them being short lived and thus not included in transport calculations. The photochemistry model is considered converged when its adaptive time step length reaches 10^{17} s within 100 time steps.

The climate model was originally developed by Kasting & Ackerman (1986), but has been significantly updated as described in Kopparapu et al. (2013) and Arney et al. (2016). Multiple studies have used this code to calculate habitable zones around a variety of stellar hosts used to study habitable zones and atmospheres of Earth-like planets around different stars (e.g., Kopparapu et al. 2013; Segura et al. 2003, 2005, 2010). The atmosphere is broken up into 100 plane parallel layers from the surface to an atmospheric pressure of 1 mbar. A correlated-k method computes the absorption of O_3, H_2O, CH_4, CO_2, and C_2H_6 throughout the atmosphere. Total absorption of incident stellar flux is calculated for each atmospheric layer with a δ-2-stream scattering algorithm (Toon et al. 1989), and outgoing IR radiation is calculated with correlated-k coefficients for each species individually. Updated H_2O cross sections from Ranjan et al. (2020) have been incorporated into the code. Convergence criteria are reached when both changes in temperature and the flux out of the top of the atmosphere are sufficiently small ($<10^{-5}$).

We run the climate and photochemistry models coupled with inputs including host stellar spectrum (121.6–45 450 nm), initial mixing ratios of atmospheric species, upper and lower boundary conditions for individual species, and initial temperature/pressure profiles. Using initial conditions the photochemistry code runs first and then transfer computed H_2O, CH_4, CO_2, and C_2H_6 mixing ratio profiles to the climate code. The climate code then updates the temperature and H_2O vapor profiles to feed back into the photochemistry. These processes iterate with profiles from the photochemistry allowing for more accurate climate code calculations and vice-versa, until a converged solution is reached.

The climate code has not been successfully run to convergence for the same atmospheric height as the photochemistry code (Arney et al. 2016), so temperature and H_2O profiles of the upper, thin part of the atmosphere (typically <60–70 km) are held constant at the highest computed value from the climate code. Sensitivity tests from Arney et al. (2016) suggest that the impact on the radiative transfer and climate of these models is not significant.

This study also implements the "short-stepping" method of convergence, as described in Teal et al. (2022). When iterating back and forth between the photochemistry and climate code, occasionally the code will oscillate between two different solutions. For example, if the photochemistry code computes a large quantity of O_3, the climate code will respond with a large amount of atmospheric heating. However, due to the temperature sensitivity of O_3 production (Reaction (2)), this hotter atmosphere will cause lower amounts of O_3 on the subsequent photochemistry iteration. Using the "short-stepping" method we do not allow the climate code to fully adjust to the updated atmospheric profiles from the photochemistry on a single iteration, and instead reach convergence slowly by iterating back and forth between the climate and photochemistry codes until a stable solution is reached.

We modeled planetary atmospheres orbiting a variety of stellar hosts (see Sect. 3.2) at the Earth-equivalent distance with varying levels of O_2. Here, we take Earth-equivalent

[1] https://github.com/VirtualPlanetaryLaboratory/atmos

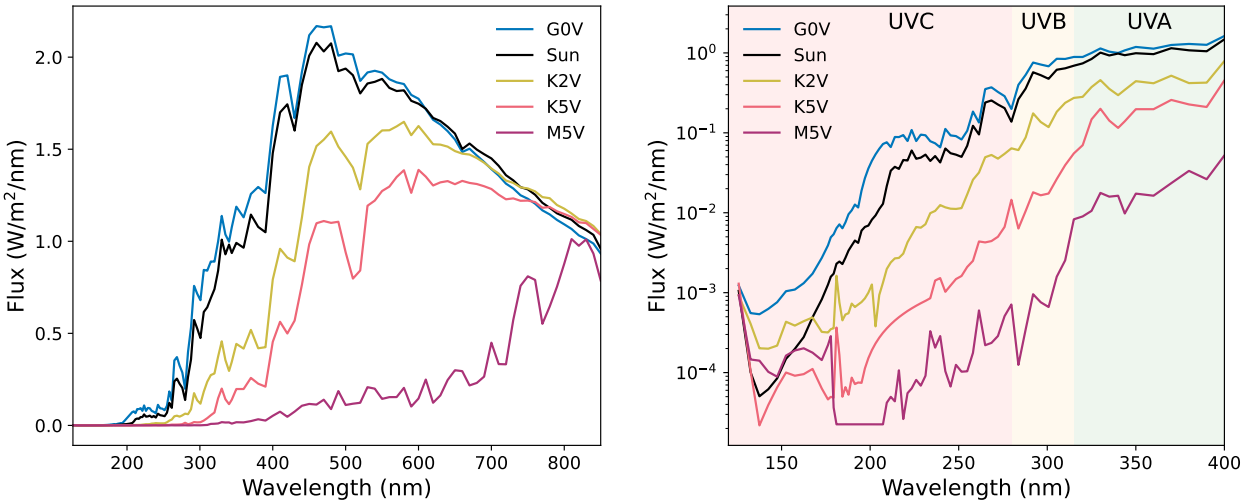

Fig. 2. Stellar spectra of the planet host stars. G0V-K5V hosts are comprised of IUE UV data from Rugheimer et al. (2013), and the M5V host comes from UV observations of GJ 876 from the MUSCLES survey (France et al. 2016). Visible and IR wavelengths use ATLAS models of the same stellar temperature (Kurucz 1979). The right-hand figure zooms in on the UV region relevant for photolysis with important biological UV regimes (see Sect. 4.4).

distance to mean that the planet receives the same total amount of incident flux from their parent stars as modern Earth receives from the Sun. We set O_2 as a constant mixing ratio for all cases, with values varying from 0.01–150% PAL O_2 (mixing ratios of 2.1×10^{-3}–0.315). Higher O_2 levels are not explored because large O_2 levels would unstable with biological compounds (Kump 2008). Lower O_2 are not modeled because it is thought that O_2 abundances from $\sim 10^{-3}$% to ~1% PAL are not expected to be stable in an Earth-like atmosphere as calculated by Gregory et al. (2021) (details on these limits in Sect. 5.4).

Other initial conditions for the models were chosen to resemble modern Earth including atmospheric mixing ratios, planetary composition, and size. `Atmos` haze production was not used. All models were run at a zenith of 60° degrees (Lambertian average) and with cloudless skies. Fixed mixing ratios were used for CH_4 (1.8×10^{-6}), N_2O (3.0×10^{-7}), and CO_2 (3.6×10^{-4}). All other species used initial atmospheric profiles and boundary conditions as defined in `Atmos`'s modern Earth template, and surface pressure remained constant at 1 bar. We note that defining CH_4 at a constant mixing ratio resembling modern Earth differs from several studies modeling "Earth-like" planets, which have adjusted CH_4 mixing ratios to reflect the CH_4 ground flux of modern Earth, resulting in much higher atmospheric CH_4 mixing ratios (e.g., Rugheimer et al. 2015a; Wunderlich et al. 2019; Teal et al. 2022). We chose to maintain CH_4 mixing ratio of modern Earth to better isolate the effects of different stellar hosts on the O_2–O_3 relationship. The impact of changing CH_4 levels on O_3 abundance is discussed further in Sect. 5.2.

3.2. Input stellar spectra

All host star spectra inputted into `Atmos` comprise of actual UV observations supplemented with synthetic ATLAS model spectra (Kurucz 1979) for the visible and IR. Table 1 contains information about the host stars and their spectra are shown in Fig. 2. The G0V-K5V stellar spectra were created in Rugheimer et al. (2013) and are a combination of UV data from the International Ultraviolet Explorer (IUE) data archives[2] and model ATLAS spectra for the same stellar temperature (Kurucz 1979).

Table 1. Stellar hosts.

Host star	Model $T_{\rm eff}$ (K)	FUV/NUV	UV data Source
G0V	6000	0.0028	a
Sun	5800	0.0010	a
K2V	5000	0.0010	a
K5V	4500	0.0012	a
M5V	3000	0.0084	b

References. a – Rugheimer et al. (2013); b – France et al. (2016).

UV data for the M5V host is from GJ 876 observations obtained by the Measurements of the Ultraviolet Spectral Characteristics of Low-mass Exoplanetary Systems (MUSCLES) survey (France et al. 2016).

The UV spectrum of a planet's host star is extremely important in the photochemical modeling of O_3 production. Not only does the total amount of UV dictate photolysis rates, but the UV spectral slope determines the creation and destruction rates of O_3. The far-UV (FUV; $\lambda < 200$ nm) is primarily responsible for photolysis of O_2 (and the creation of O_3), while the mid- and near-UV (abbreviated NUV, for brevity; 200 nm $< \lambda <$ 400 nm) is responsible for the photolysis of O_3. The NUV additionally can photolyze H_2O, which creates the HO_x species responsible for destroying O_3, causing NUV flux to destroy O_3 both directly and indirectly. Hence, a higher FUV/NUV flux ratio will create O_3 more efficiently. Low-mass, active stars tend to have lower FUV/NUV flux ratios as activity will cause excess FUV chromospheric radiation, while NUV wavelengths are often absorbed for cool stars by TiO (Harman et al. 2015).

3.3. Radiative transfer model

After `Atmos` computes the compositions of our model atmospheres, the Planetary Intensity Code for Atmospheric Scattering Observations (`PICASO`) computes planetary emission spectra (Batalha et al. 2019, 2021). `PICASO` is a publicly available[3] radiative transfer code capable of producing transmission, reflected

[2] http://archive.stsci.edu/iue

[3] https://natashabatalha.github.io/picaso/index.html

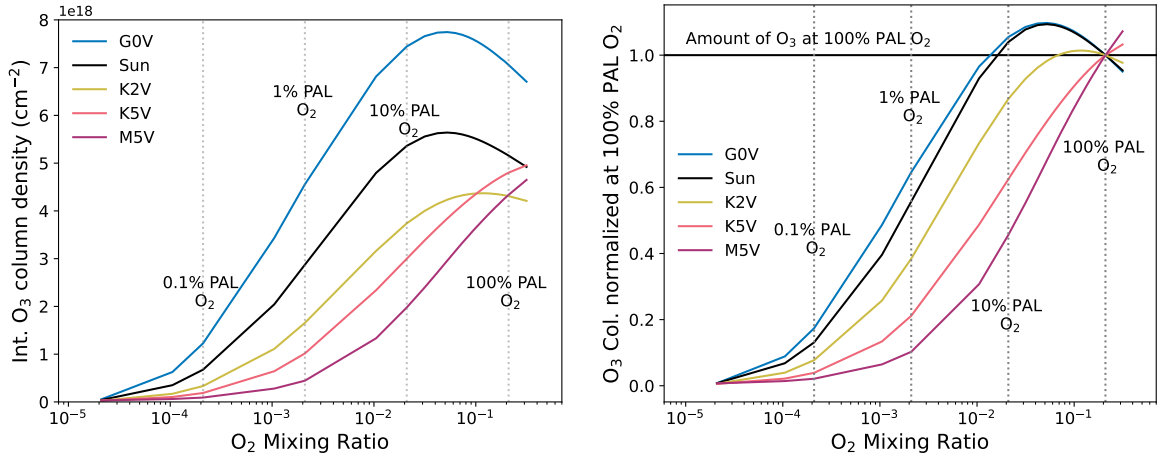

Fig. 3. O_2–O_3 relationship for Earth-like planets orbiting different host stars (indicated in legend) with varying amounts of O_2 mixing ratios. Molecular oxygen levels compared to Earth's present atmospheric level (PAL) are shown as dashed vertical lines for reference. The *left-hand* figure shows the relationship in terms of total integrated O_3 column density, and the *right-hand* figure in terms of total O_3 normalized at the amount produced in the 100% PAL O_2 case for each stellar host. The nonlinearity in these relationships is primarily due to the pressure dependence of Reaction (2) which forms O_3. The main takeaway is that the O_2–O_3 relationship is significantly different for hotter host stars (G0V, Sun, K2V) versus cooler host stars (K5V, M5V), with hotter hosts experiencing peak O_3 formation occurring at O_2 levels under 100% PAL. See Sect. 4.1 for a detailed explanation.

light, and emission spectra for a diverse range of planets. Our emission spectra were calculated at a phase angle of 0° (full phase) with altitude dependent pressure, temperature and mixing ratio profiles computed by `Atmos`. Output spectra cover a wavelength range of 0.3–14 μm, although particular focus is put on the O_3 9.7 μm feature in this study.

4. Results

4.1. O_2–O_3 relationship

Figure 3 shows the O_2–O_3 relationship for all of our model planetary atmospheres. The O_2–O_3 relationship is highly dependent on the stellar host, with different trends for model atmospheres having hotter host stars (G0V, Sun, K2V) versus cooler host stars (K5V, M5V). Since O_3 is produced via the Chapman mechanism by converting O_2 into O_3, one would naively expect the O_3 concentration to increase as the O_2 mixing ratio increases, which the case for the cooler host stars. However, the O_2–O_3 relationship for hotter stellar hosts behaves unexpectedly such that O_3 abundance peaks and then decreases as the abundance of O_2 decreases from modern Earth levels. Maximum O_3 abundance occurs in the 25% PAL O_2 models for the G0V and Sun hosts, and the 55% PAL O_2 model for the K2V host. This effect does not occur for cooler host stars, with O_3 abundance dropping consistently for models with less O_2, though not in a linear fashion. As a result, the K5V and M5V models with maximum O_2 considered (150% PAL) created the maximum amount of O_3. These results are summarized in Table 2. To allow for a simple parameterization of the O_2–O_3 relationships shown in Fig. 3 that can be used as an approximation in, for instance, GCM and retrieval modeling, we fit a fifth degree polynomial of the form,

$$y = ax^5 + bx^4 + cx^3 + dx^2 + ex + f, \quad (19)$$

where y is the integrated O_3 column density (cm^{-2}), x is the base 10 logarithm of the O_2 mixing ratio, and a, b, c, d, e, and f are the best fit polynomial coefficients listed in Table 3. This fit is valid over the range of O_2 abundances modeled in this study (0.01%–150% PAL).

Table 2. Maximum integrated O_3 column density.

Host star	Max int. O_3 Col. Density (10^{18} cm^{-2})	Max O_3 model (% PAL O_2)
G0V	7.74	25
Sun	5.64	25
K2V	4.37	55
K5V	4.96	150
M5V	4.65	150

The seemingly counterintuitive phenomenon of hotter hosts having O_3 levels increase as O_2 levels decrease can be explained by two factors: UV shielding abilities of O_2, and the pressure dependency of O_3 formation. First, we will address the UV shielding ability of O_2. Despite the fact that O_2 UV absorption cross sections are either significantly smaller than those of O_3 or require far higher energy photons (see Fig. 1), O_2 remains an important UV shield on modern Earth, primarily due to its large abundance. Although O_2 is less efficient at absorbing UV photons than O_3, O_2 makes up ~21% of the atmosphere, whereas O_3 is a trace gas with a maximum value of ~10 ppm on modern Earth. This allows the far larger number of O_2 molecules to compensate for its smaller absorption cross-sections and absorb many photons with wavelengths shorter than 240 nm (the required wavelength for O_2 photolysis, see Reaction (1)). As a result, as O_2 decreases, UV shielding in that wavelength range decreases, allowing photolysis to occur deeper in the atmosphere. This is illustrated in Fig. 4, where mixing ratio profiles of O_3, H_2O, CH_4, and N_2O are shown for all host stars at O_2 abundances of 100%, 10%, 1%, and 0.1% PAL O_2. Photolysis occurs at lower atmospheric altitudes as O_2 decreases, leading the O_3 layer to shift downward in the atmosphere. This effect is more pronounced for hotter host stars with high UV fluxes (particularly high FUV fluxes capable of O_2 photolysis), and therefore higher photolysis rates.

Secondly, the depth in which O_2 photolysis occurs is of particular importance to the altitudes at which the O_3 forming

Table 3. Coefficients of polynomial fit of the O_2–O_3 relationship.

Host star	*a*	*b*	*c*	*d*	*e*	*f*
G0V	4.582e+16	6.021e+17	2.481e+18	2.618e+18	–1.126e+18	5.742e+18
Sun	6.203e+16	7.716e+17	3.147e+18	4.157e+18	8.412e+17	4.640e+18
K2V	3.417e+16	3.846e+17	1.283e+18	7.391e+17	–8.266e+17	3.734e+18
K5V	6.826e+15	2.379e+16	–3.424e+17	–1.848e+18	–9.440e+17	4.898e+18
M5V	–2.144e+16	–3.381e+17	–1.933e+18	–4.458e+18	–1.941e+18	4.542e+18

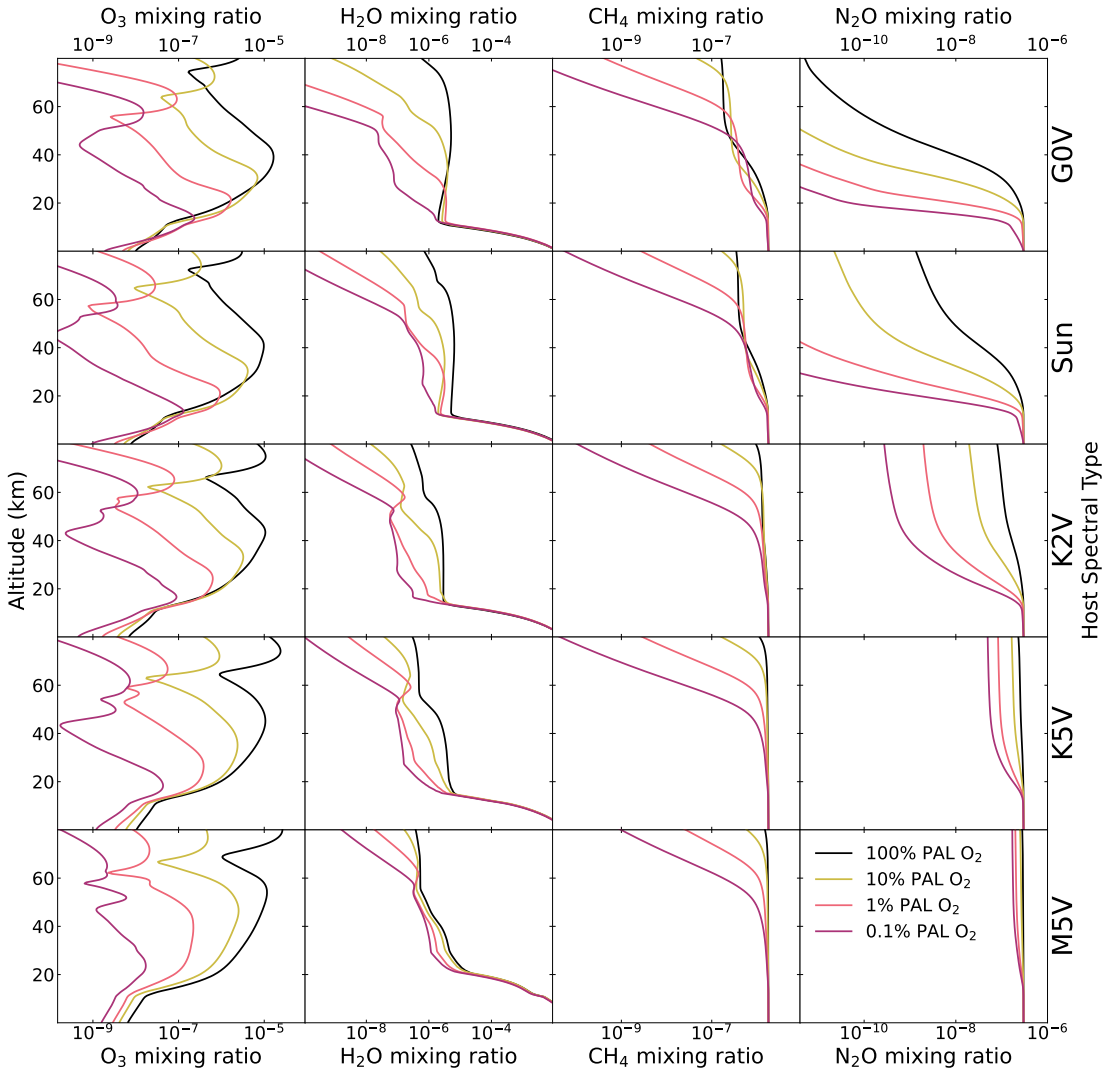

Fig. 4. Mixing ratio profiles of O_3, H_2O, CH_4, and N_2O; all potential biosignature species. Each row represents results for model atmospheres orbiting different stellar hosts as indicated on the right-hand vertical axis. Each plot shows the mixing ratio profiles for O_2 abundances of 100%, 10%, 1% and 0.1% PAL. O_2 on modern Earth is a significant UV shield, allowing model atmospheres with decreasing O_2 values to have photolysis occur at consistently lower altitudes. This is demonstrated well with the bulk of O_3 forming at lower altitudes with less O_2, as well as increased upper atmospheric depletion for H_2O, CH_4, and N_2O via photolysis. The downward shift of O_3 and upper atmospheric depletion of other species is shown to decrease for model atmospheres around cooler stars with lower incident UV flux, and hence lower photolysis rates. Full details of this atmospheric chemistry is shown in Sects. 4.1 and 4.3.

Chapman mechanism takes place, because as O_2 decreases, photolysis reaches not only deeper but also denser regions of the atmosphere. This is of significant relevance to O_3 formation due to the pressure dependency of the Chapman mechanism: Reaction (2), in which an O atom and O_2 molecule combine (with the help of a background molecule) to form O_3, is a 3-body reaction, and therefore is faster at higher atmospheric densities. Denser regions allow O, O_2, and background molecules to come together and react more rapidly than in a thinner region of the atmosphere. For hotter host stars in our sample (G0V, Sun, K2V), the UV fluxes are strong enough to allow O_2 photolysis to reach much denser atmospheric layers as O_2 decreases, allowing the benefit of faster O_3 production via Reaction (2) to outweigh the smaller source of O_2, resulting in peak O_3 abundance at lower O_2 levels.

Our cooler host stars (K5V, M5V), however, have weaker UV fluxes, meaning photons capable of O_2 photolysis cannot travel as deep in the atmosphere as for hotter hosts when O_2 decreases. The additional speed of the Chapman mechanism for lower O_2 does not make up for the smaller amount of O_2, causing O_3 abundance to decrease for decreasing O_2 abundance with these cooler host stars.

This result of an increase in O_3 production as O_2 levels decrease has been noted for the Earth-Sun system by several studies (e.g., Ratner & Walker 1972; Levine et al. 1979; Kasting & Donahue 1980; Kasting et al. 1985; Leger et al. 1993), although this is the first time it has been explored for Earth-like planets around different stellar hosts. Whether or not this would occur for an Earth-like planet will depend on if the UV flux (particularly the FUV flux) from its host star will be strong enough to incite O_2 photolysis at dense enough atmospheric levels that the increased rate of O_3 production will be enough to counter the decreased amounts of O_2 from which O_3 can form. This effect contributes to the strong dependency of the O_2–O_3 relationship on the spectral type of the host star. For example the G0V host star models have more O_3 at 10% PAL O_2 than at 100% PAL O_2, whereas for the M5V host star O_3 abundance in the 10% PAL O_2 model is nearly 60% less than it is for the 100% PAL O_2 model.

When looking at specific O_3 mixing ratios, Fig. 3 also indicates an increase in O_3 above the stratosphere for all models. This upper atmosphere O_3 (the "secondary O_3 layer") is produced primarily by O_2 photolysis from higher energy photons (>175 nm; Reaction (3)) which produces the radical $O(^1D)$. Photons of these wavelengths are absorbed high in the atmosphere but do not contribute significantly to stratospheric O_3, even when a decrease in O_2 allows photolysis to reach deeper layers of the atmosphere. Instead, these photons create O_3 above the primary O_3 layer, generally in the mesosphere and thermosphere (see Sect. 2 for more details). Although O_3 mixing ratios are high at these altitudes, due to the thin atmosphere, O_3 creation at these elevations does not add considerably to the total amount of O_3.

Also note that although the K2V host star produces enough UV photons capable of O_2 photolysis to have peak O_3 production in its 55% PAL O_2 model, both the K5V and M5V host models show a larger amount of O_3 than the K2V host for O_2 levels near 100% PAL (Fig. 3). This is because although the K2V host has more FUV than the K5V and M5V hosts (Fig. 2), the cooler hosts have higher FUV/NUV ratios (Table 1), allowing more efficient O_3 production without as much NUV O_3 destruction.

In summary, the O_2–O_3 relationship is highly dependent on the UV flux of the host star, with different trends for hotter and cooler host stars. Hotter host stars with high FUV fluxes experience peak O_3 abundance at lower O_2 levels due to O_3 formation occurring in deeper, denser parts of the atmosphere where the Chapman mechanism is more efficient. Cooler host stars do not emit enough FUV flux for this effect to occur, and experience consistently decreasing O_3 as O_2 decreases.

4.2. Impact of varying O_2 on H_2O, CH_4, and N_2O

Figure 4 shows the impact of varying O_2 levels on the biologically relevant atmospheres species H_2O, CH_4, and N_2O. As O_2 decreases, photons usually absorbed by O_2 ($\lambda < 240$ nm) travel deeper into the atmosphere and drive the majority of atmospheric changes. This allows photolysis in general to reach lower altitudes, as well as photolysis caused by high energy photons that create the $O(^1D)$ radical, which reacts quickly with many species. $O(^1D)$ is produced via photolysis of O_2, O_3, N_2O, and CO_2 as follows:

$$O_2 + h\nu \rightarrow O + O(^1D)\ (\lambda < 175\ \text{nm}), \quad (3)$$

$$O_3 + h\nu \rightarrow O_2 + O(^1D)\ (\lambda < 310\ \text{nm}), \quad (5)$$

$$N_2O + h\nu \rightarrow N_2 + O(^1D)\ (\lambda < 200\ \text{nm}), \quad (20)$$

$$CO_2 + h\nu \rightarrow CO + O(^1D)\ (\lambda < 167\ \text{nm}). \quad (21)$$

As O_2 decreases, $O(^1D)$ creation moves deeper into the atmosphere for all these species. For our models, O_3 photolysis consistently creates the most $O(^1D)$, particularly at lower atmospheric heights. O_2 photolysis is also a significant producer of $O(^1D)$, although it is limited to the stratosphere and above, even for the lowest O_2 levels modeled in this study. CO_2 and N_2O photolysis contribute to $O(^1D)$ production as well, although CO_2 photolysis is constrained to the upper atmosphere similarly to O_2 photolysis, while N_2O photolysis can occur much closer to the planetary surface for low O_2 levels. Increased rates of photolysis as O_2 shielding decreases as well as increased $O(^1D)$ production reaching lower atmospheric levels causes the depletion of many species.

H_2O is increasingly depleted for decreasing levels of O_2 due to both photolysis in the atmosphere and $O(^1D)$ reactions lower in the atmosphere. Both of these reactions create the OH radical while removing H_2O,

$$H_2O + h\nu \rightarrow H + OH, \quad (22)$$

$$H_2O + O(^1D) \rightarrow OH + OH. \quad (8)$$

On modern Earth, Reaction (8) is the primary source of OH in the stratosphere, which is a major sink for several species. As H_2O levels in the upper atmosphere drop with decreasing O_2, this causes OH production to move to lower levels of the atmospheres as seen in Fig. 5. Upper atmospheric depletion of H_2O and OH production at lower altitudes is seen more strongly for hotter host stars, as they have higher incident UV for photolysis and $O(^1D)$ creation.

CH_4, an important biosignature gas, is also depleted in the upper atmosphere for models around all host stars, primarily though oxidation via OH (created via reactions with H_2O), along with photolysis and reactions with $O(^1D)$,

$$CH_4 + OH \rightarrow CH_3 + H_2O, \quad (23)$$

$$CH_4 + O(^1D) \rightarrow CH_3 + OH. \quad (24)$$

In the upper atmosphere, depletion is dominated by photolysis. Reaction (23) is both the main sink of stratospheric CH_4 and OH depletion on modern Earth, with CH_4 and OH acting as a major sinks for each other. Reactions with $O(^1D)$ and OH occur deeper in the atmosphere for decreasing O_2 levels as both these radicals are produced at lower altitudes. Reaction (24) is an additional source of OH in the lower stratosphere/troposphere. CH_4 depletion is limited to the upper stratosphere for model atmospheres around cooler hosts, although can reach the lower stratosphere for model atmospheres with hotter hosts.

N_2O, another potential biosignature gas, experiences extreme depletion for hotter hosts down to the troposphere for lower levels of O_2, and significantly less depletion constrained to the upper atmosphere around cooler stars. This is due primarily to photolysis (Reaction (20)) in the upper atmosphere, although there are contributions from interactions with $O(^1D)$ as well,

$$N_2O + O(^1D) \rightarrow NO + NO. \quad (14)$$

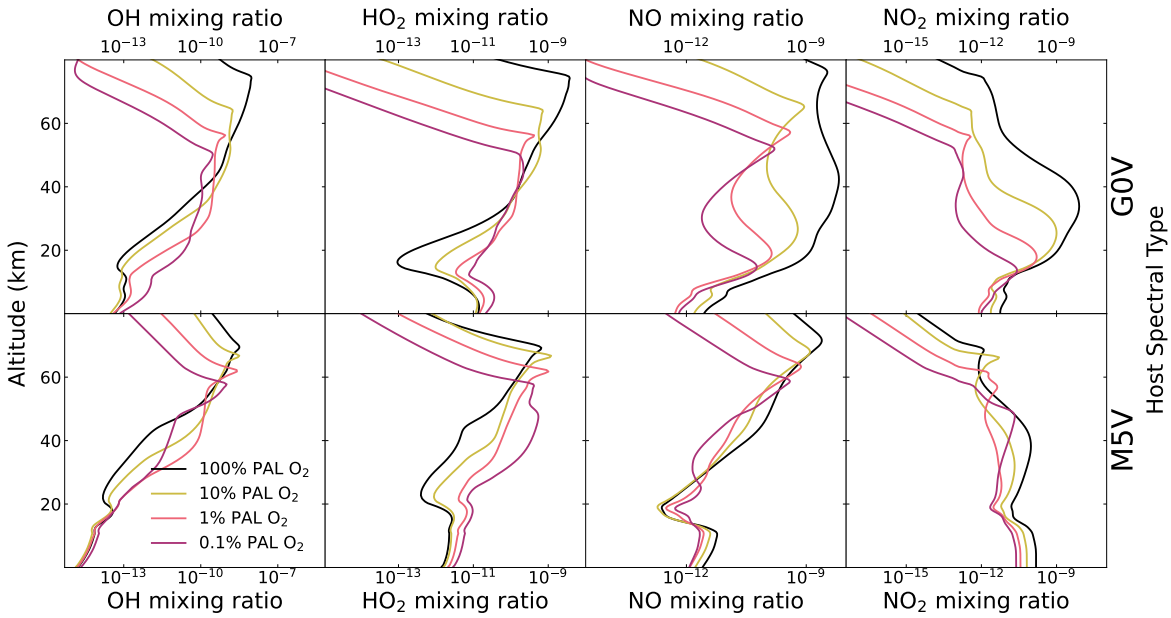

Fig. 5. Mixing ratio profiles of HO_x (OH + HO_2) and NO_x (NO + NO_2) species that power the catalytic cycles which destroy O_3 for models with 100%, 10%, 1%, and 0.1% PAL O_2. Here, we show models for the hottest (G0V) and coolest (M5V) stellar hosts. For decreasing O_2 levels photolysis reaches lower levels of the atmosphere, causing OH and HO_2 formation to occur at lower levels. The HO_x is not significantly impacted by these changes since O_3 formation is pushed deeper into the atmosphere as well. NO_x species experience depletion via N_2O and NO photolysis, although are less affected for models around cooler stars with lower photolysis rates. The efficiency of the NO_x catalytic cycle decreases consistently for all host stars with decreasing O_2 levels. See Sect. 4.3 for full details.

Depletion rates of N_2O vary significantly between different stellar hosts due to the strong dependence of incident UV flux on N_2O destruction.

In summary, the majority of changes to an atmosphere as O_2 decreases are caused by increased photolysis rates as O_2 UV shielding decreases as well as $O(^1D)$ production from either O_2, O_3, N_2O, or CO_2 photolysis occurring at lower levels of the atmosphere. These effects cause upper atmospheric depletion of H_2O, CH_4, and N_2O, with more depletion for hotter stellar hosts with stronger UV fluxes.

4.3. Impact of varying O_2 on catalytic cycles

Varying O_2 levels impacts HO_x (OH + HO_2) and NO_x (NO + NO_2) species, which are the main contributors of catalytic cycles that destroy O_3 (see Sect. 2.2 for details). Mixing ratio profiles of these species are shown in Fig. 5 for our hottest and coolest host stars. Once again, the impact on these species as O_2 levels are decreased is controlled by photolysis reaching deeper levels of the atmosphere along with $O(^1D)$ production moving to lower levels as well.

As O_2 decreases, HO_x species (OH and HO_2) in all models decrease in the upper atmosphere, but increase in the lower atmosphere. OH production via reactions with H_2O (Reactions (8), (22)) and CH_4 (Reaction (24)) occur at lower altitudes for lower O_2 levels, especially since both H_2O and CH_4 are depleted in the upper atmosphere from photolysis. This "pushing down" of HO_x species is more noticeable for hotter host stars with higher photolysis rates. Also note that stars with lower FUV/NUV ratios can better remove O_3 via the HO_x catalytic cycle, as FUV wavelengths create O_3, while NUV wavelengths photolyze H_2O to form OH. However, for all host stars the efficiency of the HO_x catalytic cycle of O_3 destruction is not largely impacted for different O_2 and O_3 abundances since OH and HO_2 move down in the atmosphere along with O_3 concentrations. Decreased O_2 UV shielding and increased photolysis does not destroy HO_x species, but rather converts them into other HO_x species. When HO_2 is photolyzed,

$$HO_2 + h\nu \rightarrow OH + O, \quad (25)$$

it creates OH. The OH radical itself is extremely reactive with a short lifetime, and typically will react quickly with other species or react with O_3 to create HO_2 (Reaction (9)).

Although with decreasing O_2 abundance HO_x species are formed lower in the atmosphere rather than destroyed by photolysis, NO_x species (NO + NO_2) can be depleted via photolysis. The main source of NO_x in the stratosphere is via N_2O reactions with $O(^1D)$. However, as shown in Fig. 4, N_2O is significantly depleted in the atmosphere via photolysis, especially for hotter host stars. While H_2O, the primary source of HO_x species in the stratosphere creates HO_x during photolysis, N_2O, the primary source of NO_x species, does not. Instead it creates N_2 and $O(^1D)$ (Reaction (20)), cutting off the main source of NO production from N_2O. As for NO_x species themselves, NO_2 photolysis creates more NO, while NO photolysis simply breaks the molecule apart,

$$NO_2 + h\nu \rightarrow NO + O, \quad (26)$$
$$NO + h\nu \rightarrow N + O, \quad (27)$$

causing NO photolysis to be a sink of NO_x. NO can be formed once again via reactions between N atoms and O_2 molecules,

$$N + O_2 \rightarrow NO + O, \quad (28)$$

although the rate of NO photolysis is faster than Reaction (28), causing it to be a gradual sink of NO_x. Often the N atom created by Reaction (27) will remove NO_x via,

$$NO + N \rightarrow N_2 + O, \quad (29)$$

Table 4. UV integrated fluxes.

Spectral	O_2 MR	UVA 315–400 nm (W m^{-2})			UVB 280–315 nm (W m^{-2})			UVC 121.6–280 nm (W m^{-2})		
Type	(% PAL)	TOA	Surface	% to surf.	TOA	Surface	% to surf.	TOA	Surface	% to surf.
G0V	100	96.6	77.9	80.7	22.4	1.5	6.7	11.2	3.8e–27	3.4e–26
G0V	10	96.6	76.7	79.4	22.4	1.4	6.2	11.2	1.8e–08	1.6e–07
G0V	1	96.6	77.5	80.3	22.4	2.4	10.7	11.2	1.7e–04	1.5e–03
G0V	0.1	96.6	78.6	81.4	22.4	5.9	26.3	11.2	1.7e–02	1.5e–01
Sun	100	82.9	67.5	81.4	16.2	1.6	10.2	6.7	2.8e–21	4.1e–20
Sun	10	82.9	66.5	80.2	16.2	1.6	9.6	6.7	3.3e–08	5.0e–07
Sun	1	82.9	67.1	81.0	16.2	2.7	16.4	6.7	2.3e–04	3.5e–03
Sun	0.1	82.9	67.7	81.7	16.2	5.6	34.8	6.7	1.5e–02	2.3e–01
K2V	100	34.2	28.0	81.9	4.8	0.68	14.1	1.4	1.1e–18	8.0e–17
K2V	10	34.2	27.6	80.8	4.8	0.74	15.4	1.4	1.8e–08	1.3e–06
K2V	1	34.2	27.8	81.4	4.8	1.2	25.4	1.4	1.0e–04	7.3e–03
K2V	0.1	34.2	28.0	81.8	4.8	2.2	44.8	1.4	1.0e–02	7.2e–01
K5V	100	15.3	12.8	83.6	0.68	0.10	14.4	0.16	2.1e–21	1.3e–18
K5V	10	15.3	12.6	82.6	0.68	0.14	20.1	0.16	8.4e–09	5.1e–06
K5V	1	15.3	12.7	82.9	0.68	0.23	33.6	0.16	5.4e–05	3.3e–02
K5V	0.1	15.3	12.7	83.0	0.68	0.34	50.4	0.16	4.7e–03	2.8e+00
M5V	100	1.6	1.3	83.8	3.5e–02	6.5e–03	18.4	2.7e–02	9.8e–21	3.6e–17
M5V	10	1.6	1.3	83.1	3.5e–02	1.0e–02	28.8	2.7e–02	4.1e–09	1.5e–05
M5V	1	1.6	1.3	83.4	3.5e–02	1.6e–02	45.7	2.7e–02	3.8e–05	1.4e–01
M5V	0	1.6	1.3	83.4	3.5e–02	2.0e–02	56.3	2.7e–02	1.1e–03	4.2e+00

Notes. Abbreviations: MR = mixing ratio; PAL = present atmospheric level; TOA = top of atmosphere.

or the N atoms will recombine with other N atoms,

$$N + N \rightarrow N_2, \tag{30}$$

with this reaction becoming more efficient as O_2 levels drop. This sink via NO photolysis has less of an impact on cooler host stars with lower photolysis rates, hence less NO_x depletion.

As seen in Fig. 5, NO_x species are depleted throughout the atmosphere for the G0V host star, while the M5V host star experiences less NO_x depletion, and actually an increase in NO in the lower stratosphere. This is due to primarily to lower photolysis rates for the cooler M5V star which depletes less N_2O and NO (Reaction (14)). However, for model atmospheres around all host stars the ability of the NO_x catalytic cycle to deplete O_3 diminishes consistently with decreasing O_2 levels, even for cooler stellar host models with less NO_x depletion.

In summary, the HO_x catalytic cycles are not hugely impacted by decreasing O_2 because increased photolysis rates tend to push HO_x species to lower altitudes rather than destroy them. However, NO_x catalytic cycles decrease in efficiency with lower O_2 levels since photolysis of N_2O and NO remove NO_x from the atmosphere.

4.4. Surface UV flux for different O_2 and O_3 levels

`Atmos` was used to calculate the amount of UV flux reaching the planetary surface in each model atmosphere. Surface UV flux is strongly dependent on incident stellar UV flux and the amount of UV shielding from both O_2 and O_3. High UV fluxes can cause substantial damage to biological organisms, hence UV surface environments will be critical for determining surface habitability. These results are summarized in Table 4 and shown in Fig. 6. Surface UV fluxes calculated here using a zenith angle of 60° (see Sect. 3.1).

Integrated surface UV fluxes are broken up into three biologically relevant wavelength regimes: UVA, UVB, and UVC. UVA flux (315–400 nm) is the lowest energy type of UV and is only partially shielded by O_3, so a large percentage of incident UVA on modern Earth reaches the planetary surface. UVB (280–315 nm) is more harmful for life, contributing to sun burn and skin cancer in humans and damage to other organisms (e.g., Kiesecker et al. 2001). UVB is shielded much more efficiently by O_3 than UVA, with a smaller fraction of incident UVB reaching the surface of modern Earth. UVC (121.6–280 nm) is capable of causing DNA damage, but is fortunately shielded almost entirely by O_3 on modern Earth. Ozone is most efficient at shielding UV in this wavelength region, as evidenced by the O_3 absorption cross sections shown in Fig. 1. We note that O_2 photolysis, the first step in O_3 formation (Reactions (1), (3)), requires a UVC photon ($\lambda < 240$ nm), allowing O_2 to contribute partially to UVC shielding. However, since O_3 is the primary shielder of UVC, the requirement of a UVC photon to produce O_3 creates interesting correlations between incident and surface UVC flux.

Because UVA is not strongly shielded by O_3, UVA surface fluxes for all models are closely correlated with the amount of incident UVA flux (see Table 4 and Fig. 6). For all host stars at O_2 levels of 100%, 10%, 1%, and 0.1% PAL the amount of incident UVA that reaches the surface of these model planets is roughly ~80% for all cases. Because O_3 plays only a small role in UVA shielding, all model results are quite similar.

UVB surface fluxes are significantly more variable because O_3 shielding is much more important for these wavelengths. Although the G0V host star provides a higher incident UVB flux than the Sun, G0V-hosted models still maintain slightly less surface UVB flux until O_2 decreases to 0.1% PAL, at which point the G0V and Sun model surface fluxes become roughly equal. This is due to the larger amount of O_3 created by the G0V

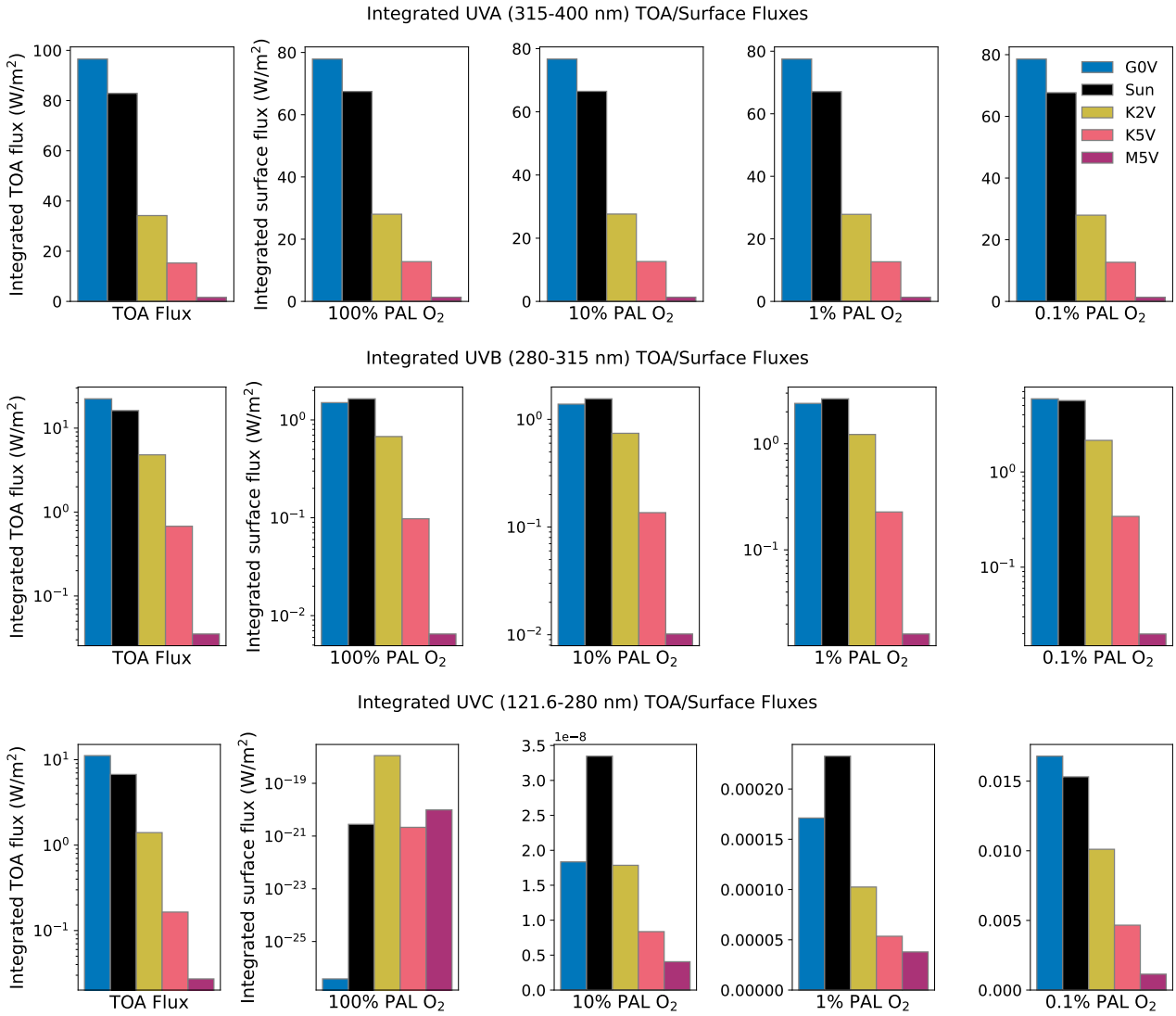

Fig. 6. Top-of-the atmosphere (TOA) and surface fluxes for UVA (*top*), UVB (*middle*), and UVC (*bottom*) wavelengths for 100%, 10%, 1%, and 0.1% PAL O_2 model atmospheres for all stellar hosts. We note the differences in y-axis scale for different subplots. UVA flux is only slightly shielded by O_3 so surface fluxes scale roughly with TOA fluxes. UVB flux is partially shielded by O_3 and therefore allows the G0V-hosted models to receive less surface UVB than Sun-hosted models despite higher TOA UVB due to more efficient O_3 production. UVC surface fluxes for high O_2 levels are strongly influenced by O_3 abundance due to strong UV shielding from O_3 in this wavelength range. For models with only 0.1% PAL O_2 levels all surface UV fluxes begin to converge to TOA values as the shielding of O_3 is significantly decreased. See Sect. 4.4 for full details.

host star compared to the Sun, which allows for stronger UVB shielding (see Fig. 3 for O_2–O_3 relationship). The percentage of incident UVB flux that reaches the planetary surface varies significantly between different host stars. For our hottest host star (G0V) the amount of incident UVB flux reaching the planetary surface increases from 6.7% to 26.3% as O_2 levels drop from 100% to 0.1% PAL. As a result of less O_3 shielding, these percentages are higher for our coolest host star (M5V), which experiences an increase of 18.4% to 56.3% of incident UVB reaching the surface as O_2 decreases from 100% to 0.1% PAL. Even though the cooler stellar hosts allow a higher percentage of UVB flux to travel through the atmosphere, they still maintain lower surface UVB values than hotter hosts due to their weaker incident UVB flux.

The strong reliance of UVC absorption on O_3 abundance, along with the fact that O_3 creation requires UVC photons, leads to some unexpected UVC surface flux results. A striking consequence of this is that while the G0V host star provides the highest incident UVC flux of all our host stars, it maintains the lowest surface UVC flux for the 100% PAL O_2 model by several orders of magnitude, while the much cooler K2V stellar host model experiences the highest surface UVC flux. The much higher incident UVC flux of the G0V host causes much faster O_3 production than other host stars, allowing for UVC shielding strong enough to counteract the high incident UVC flux. Another interesting result for the 100% PAL O_2 case is that the M5V model has a slightly higher UVC surface flux than the K5V model, despite the fact that the M5V model has the lowest incident UVC flux. Again, this effect is due to the higher O_3 abundance of the K5V-hosted planet, created by the stronger incident UVC flux. For all host stars, the atmospheric models with 100% PAL O_2 allowed only extremely tiny fractions of incident UVC flux reach the surface ($<10^{-17}$% in all cases).

UVC surface fluxes for models with 10% and 1% PAL O_2 have similar trends when comparing stellar hosts. Sun-hosted models had the largest surface UVC fluxes in both scenarios.

Notice that although the model atmospheres hosted by the G0V star and the Sun have higher O_3 levels for the 10% PAL O_2 cases compared to their 100% PAL O_2 cases, overall UVC shielding is significantly less for the 10% PAL O_2 cases due to the lesser contribution of O_2 absorbing photons with wavelengths less than 240 nm. Even though the G0V host and the Sun produce much larger amounts of O_3 than cooler stars, for low O_2 levels the combined decrease in O_2 and O_3 UV shielding causes them to have higher surface UVC fluxes than cooler stars that produce significantly less O_3. For model atmospheres with O_2 levels of only 0.1% PAL, surface UVC levels begin to converge to the incident UVC flux as O_2 and O_3 levels have dropped enough that they shield UVC far less effectively. It has previously been suggested that the usefulness in the ability of O_3 to shield UV drops off drastically at these O_2 values (e.g., Segura et al. 2003). However, due to CO_2 shielding, all models in this study had virtually no photons with wavelengths less than 200 nm reach the planetary surface, even with the lowest O_2 abundance modeled (0.01% PAL).

Although the model atmospheres hosted by the hottest stars create the highest levels of O_3, they constantly experience the highest UVA and UVB surface fluxes due to the limited shielding abilities of O_3 in these wavelength ranges. However, for the far more damaging UVC wavelengths at 100% PAL O_2 it is the G0V host star that provides the lowest UVC surface flux by orders of magnitude, with the Sun-hosted models having comparable UVC surface flux to cooler host star models. Somewhat ironically, for lower O_2 levels of 1–10% PAL, it is the Sun that is the host star with the least "hospitable" conditions for surface life with the highest UVC surface fluxes. As O_2 drops to 0.1% PAL UVC surface flux will begin to converge to the incident UVC flux as O_2 and O_3 shielding drops dramatically. However, though life on modern Earth requires a substantial O_3 layer for UV protection, it is important to remember that evidence for life on Earth dates back to 3.7 Gyr ago (Rosing 1999), long before the O_2 levels rose during the Great Oxidation Event 2.5 Gyr ago. The lack of significant atmospheric UV shielding may prevent life as we know it, but it does not rule out its existence. Life could exist, for instance, underwater, at a depth in which significant damaging UV has been absorbed by water (e.g., Cockell & Raven 2007).

4.5. O_3 spectral features for different O_2 levels

Emission spectra from our model atmospheres are shown in Fig. 7, zoomed in on the primary MIR O_3 feature at 9.7 μm, along with the corresponding O_3 mixing ratio and temperature profiles, which are necessary for interpreting the features. The temperature difference between the absorbing and emitting layers of the planet's atmosphere, rather than the overall abundance of that gaseous species, determines the depth of planetary emission spectrum features. Because O_3 is a main contributor of stratospheric heating, the strength of O_3 features has a highly nonlinear relationship to O_3 abundance. Once again, we see counterintuitive trends for hotter host stars (G0V, Sun, K2V), and different, more straightforward trends, for cooler host stars (K5V, M5V).

For all host stars, the 0.1% PAL O_2 case has the shallowest O_3 feature in emission spectra, but the O_2 level for the deepest feature depends on the host star. For the G0V-hosted models the O_3 feature for the 100% PAL O_2 case has a similar depth to the 0.1% PAL O_2 case, despite the fact that they have significantly different integrated O_3 column densities (7.06×10^{18} cm^{-2} for 100% PAL O_2; 1.23×10^{18} cm^{-2} for 0.1% PAL O_2). For the two hottest host stars (G0V, Sun), the 10% and 1% PAL O_2 cases are the deepest features. The strong features of the 10% PAL O_2 models are not surprising since both the G0V and Sun models have higher O_3 abundances at 10% PAL than at 100% PAL O_2, but the 1% PAL O_2 models have significantly less O_3 than both the 10% and 100% PAL O_2 cases (see Fig. 3 for reference). Conversely, O_3 features for the coolest host star models correspond more intuitively to O_2 and O_3 levels, with the highest O_2 and O_3 abundances having the deepest features, and the lowest O_2 and O_3 abundances having the shallowest features.

The relationship between the depth of O_3 spectral features and actual O_3 abundance is dictated by atmospheric temperature profiles. The temperature difference between the emitting and absorbing layers of a gaseous species determines feature depth, therefore O_3 feature depth is determined by the temperature difference between the altitude of peak O_3 concentration in the stratosphere and the planet's surface temperature. Because O_3 NUV absorption is a dominant source of stratospheric heating, a higher O_3 concentration with significant incident NUV flux for O_3 to absorb results in higher stratospheric temperatures and thus a shallower spectral feature. This explains why an atmosphere with a large amount of O_3 and high incident NUV flux (and more stratospheric heating) has a weaker O_3 feature than an atmosphere with less O_3 and weaker incident NUV, but a larger temperature difference between the stratospheric and surface temperatures. Cooler host star models with less O_3 formation and lower incident NUV flux have significantly less stratospheric heating (Fig. 7), and therefore O_3 spectral feature depths which correspond more strongly with the actual abundance of O_3 in their atmospheres.

In summary, in order to interpret O_3 features in planetary emission spectra and retrieve the O_3 (and O_2) abundances it will require modeling of the atmospheric temperature profiles. Both photochemistry and climate modeling will be essential in this process.

5. Discussion

5.1. Comparison to other studies

Multiple studies have explored O_3 formation in Earth-like atmospheres using a variety of models, each providing valuable insight on the O_2–O_3 relationship. Here, we briefly describe relevant past studies on this topic. With 1D modeling of Earth's atmosphere, early O_3 studies revealed the nonlinear link between O_3 and O_2. Both Ratner & Walker (1972) and Levine et al. (1979) discuss the phenomenon of the O_3 layer moving down in the atmosphere as O_2 levels decreased (see Sect. 4.1 for details on this process) and agreed on peak O_3 abundance occurring at ~10% PAL O_2. Total O_3 abundances calculated for these studies differed because they each included different chemical reactions. The model in Ratner & Walker (1972) contained only the Chapman mechanism, while Levine et al. (1979) additionally HO_x and NO_x catalytic cycle destruction of O_3 in their model. Later Kasting et al. (1985) replicated the O_3 peak in abundance at lower O_2 levels using a more sophisticated model including chemistry beyond the Chapman mechanism and catalytic cycles, incorporating 20 gaseous species overall. They predicted maximum O_3 production to occur at 50% PAL O_2, a higher O_2 estimate than previously. It is important to note that none of these studies included a climate model to calculate self-consistent atmospheric temperatures. Because the Chapman mechanism is temperature dependent, this helps account for discrepancies with later O_3 calculations.

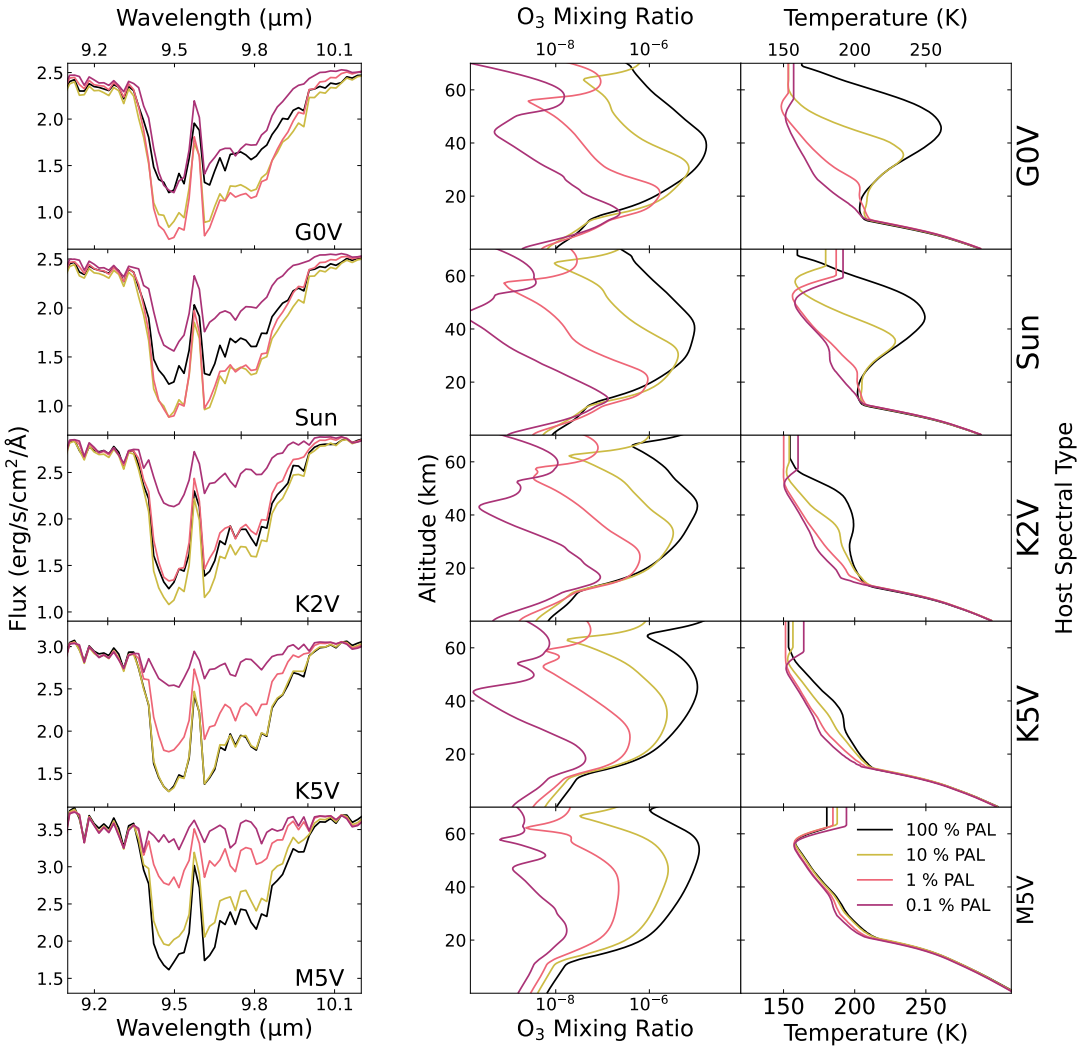

Fig. 7. Emission spectra, O_3 mixing ratio profiles, and temperature profiles for model atmospheres with 100%, 10%, 1%, and 0.1% PAL O_2 for all host stars. The depth of spectral features in emission spectra is dependent on the temperature difference between the absorbing and emitting layers of the atmosphere, causing the O_3 feature depth to strongly correlate with the temperature difference between the stratosphere and planetary surface. However, since O_3 is responsible for the majority of stratospheric heating, this results in higher O_3 abundances (with more stratospheric heating) having shallower spectral features than atmospheres with less O_3 and cooler stratospheres. For full details see Sect. 4.5. We note that temperatures for parts of the atmosphere above 1 mbar are held constant as that is the maximum height computed by the climate code (see Sect. 3.1 for more details).

Studies in later years began to model O_3 production in planetary atmospheres with different types of host stars. Segura et al. (2003) used what they described as a "loosely coupled" 1D climate and photochemistry code (partially based off the Kasting et al. 1985 model) for different O_2 levels around F2V, G2V, and K2V type stars. We note that this model is a predecessor of the model used in this study: `Atmos`. No host star displayed a peak O_3 abundance at an O_2 level less than 100% PAL, but this is likely because the modeled O_2 levels were evenly spaced on a logarithmic scale from 0.001–100% PAL O_2, whereas more finely spaced O_2 levels are required to capture this effect. Atmospheric chemistry and temperature profiles computed in Segura et al. (2003) are similar to our Sun and K2V host star models. There are slight differences in total O_3 abundance in these models compared to those in this study (our models tend to have lower O_3), although this is likely due to differences in input UV spectra, boundary conditions, and model updates. Overall this is the most similar study to ours in terms of variety of O_2 levels and host stars.

Other studies have also modeled O_3 formation in Earth-like planetary atmospheres around different stellar hosts. The effect of varying orbital separations inside the habitable zone on O_3 formation was explored for F2V, G2V, and K2V hosts (same as Segura et al. 2003) in Grenfell et al. (2007), and for a variety of M dwarfs in Grenfell et al. (2014). Both these studies used the 1D "loosely coupled" climate and photochemistry model developed in Segura et al. (2003). An increase in star–planet separation for FGK stars caused cooler atmospheric temperatures, which correlated to an increase in O_3. This is because the 3-body reaction that creates O_3 (Reaction (2)) is faster at cooler temperatures. However, this O_3 increase was not large because larger orbital distances also caused higher levels of HO_x and NO_x species which destroy O_3 (Grenfell et al. 2007). When repeating this study for M dwarfs they found what they described as a "Goldilocks" effect in which there was a range of UV that was best for creating the most detectable O_3. If incident UV flux is too low it will create small amounts of O_3 making it harder to detect, but if the UV flux is too high it will create enough O_3 to

cause significant stratospheric heating, making it more difficult to detect in planetary emission spectra (see Sect. 4.5 details on this phenomenon). M7V spectral types were found to produce the amount of UV that was "just right" in creating detectable amounts of O_3 (Grenfell et al. 2014). Although these models were run only at 100% PAL O_2, their results are consistent with this study.

The impact of stellar host UV on O_3 formation has also been modeled using *Exo-Prime*, a 1D coupled climate and photochemistry originally based off the same codes as `Atmos`, for Earth-like planets orbiting FGKM stars (Rugheimer et al. 2013), M dwarfs (Rugheimer et al. 2015a), cool white dwarfs (Kozakis et al. 2018), and red giants (Kozakis & Kaltenegger 2019). However, all these studies were constrained to O_2 abundances of 100% PAL, although our corresponding models results are consistent. Another *Exo-Prime* study (Rugheimer et al. 2015b) modeled Earth at different points throughout geological history for FGKM stars, including four different O_2 abundances, although the large variations in abundances of many gaseous species (i.e., CH_4, CO_2) does not allow for a straightforward comparisons of results with our study.

Of the 1D models discussed in this study, only `Atmos` models photochemistry in the mesosphere and lower thermosphere (up to an altitude of 100 km), whereas other photochemistry models are limited to atmospheric heights below ~65 km (Kasting & Donahue 1980; Kasting et al. 1985; Segura et al. 2003; Grenfell et al. 2007, 2014; Rugheimer et al. 2013, 2015a,b; Kozakis et al. 2018; Kozakis & Kaltenegger 2019). This is relevant for O_3 formation because of the "secondary O_3 layer" on Earth above the stratosphere (see details in Sects. 2 and 4.1). High energy photons ($\lambda < 175$ nm) are normally absorbed above the stratosphere by O_2 photolysis, creating the $O(^1D)$ radical in the process (Reaction (3)). This could yield different findings for a photochemistry model that does not include higher altitudes since the high-energy photons will then be absorbed at far lower altitudes than in reality. This would change both the $O(^1D)$ and O_3 atmospheric profiles, and account for the differences in O_3 production the we see from different models. However, overall results from the Segura et al. (2003) model, *Exo-Prime*, and `Atmos` remain fairly consistent.

Along with 1D models, O_3 formation has been modeled in 3D. In reality, O_3 formation and abundance is dependent on both the atmospheric latitude and time of day. On the night side of a planet, O_3 cannot be generated by the Chapman method nor destroyed by photolysis. During the day O_3 is created most efficiently at the equator where incident UV flux is highest, and then is transported toward the poles by Dobson-Brewer circulation, causing peak O_3 abundance to vary in altitude depending on the latitude. On modern Earth, there is only a ~2% difference in O_3 between the day and night sides, while planets with differing rotation periods may have more unevenly distributed O_3. Despite the fact that 1D models (like ours) can use a zenith angle to represent the "average" of incoming radiation, they cannot accurately predict O_3 formation and transport for slowly rotating planets, especially ones that are tidally-locked. Several studies have used 3D modeling to explore O_3 formation and distribution on tidally locked planets. Proedrou & Hocke (2016) used a 3D climate and photochemistry model to compare O_3 distribution on modern Earth and a tidally-locked version of Earth. They found that O_3 could be distributed to the night-side of the planet and accumulate there in the absence of photolysis. Hemispheric maps of O_3 distribution at different phases demonstrated that the amount of detectable O_3 will be phase-dependent during observations.

Tidally-locked Earth-like planets are most likely found around lower mass stars, where the tidal-locking radius is within the habitable zone, and rotation periods are substantially shorter than the "tidally-locked Earth around the Sun" scenario investigated in Proedrou & Hocke (2016). Carone et al. (2018) used a 3D GCM to model how the rapid rotation of a tidally-locked planet would affect O_3 transport on a planet with a 25-day period. This faster rotation created an "anti-Dobson-Brewer circulation" effect, with O_3 accumulating at the equator rather than being transported toward the poles as on modern Earth. However, this study did not employ a photochemistry model, only circulation effects.

Chen et al. (2018) and Yates et al. (2020) also performed 3D modeling of tidally-locked habitable zone planets orbiting M dwarfs, although they incorporated both climate and photochemistry models as well. Chen et al. (2018) used CAM-Chem, a 3D model including 97 species in chemistry computations, while Yates et al. (2020) used the Met Office Unified Model including only Chapman mechanism and HO_x catalytic cycle chemistry. Both studies found that O_3 would be transferred to the night-side after being created on the day-side, where it could accumulate to a higher quantity than on the day-side. HO_x species that were also transported to the night-side would be the primary sink of night-side O_3. However, Yates et al. (2020) computed a thinner O_3 layer than Chen et al. (2018), with the latter's model also computing that O_3 would exist at higher altitudes. These differences are likely due to differing chemical networks, land mass fraction (only Chen et al. 2018 had continents), and input stellar spectra. Overall these results agreed well with O_3 abundances calculated by Rugheimer et al. (2015a) for a similar host star, although H_2O mixing ratios (important for creating HO_x species) were shown to vary significantly more, showing that 1D models do not include important feedback loops contained within 3D models.

The closest similar 3D modeling work to ours is Cooke et al. (2022), which uses a 3D climate-chemistry code to model the Earth-Sun system across geological history at various O_2 levels from 0.1% to 150% PAL. Comparing their results to our Sun-hosted models there is agreement between trends in the time-averaged mixing ratios for different gaseous species. However, a main finding of Cooke et al. (2022) is that their 3D model predicts lower O_3 abundances for O_2 levels 0.5% to 50% PAL when compared to 1D models, including those calculated here as well as in Segura et al. (2003) and Rugheimer et al. (2015b). The cause for these lower estimates from this 3D model is uncertain, although is possibly related to how 1D codes simulate diurnal averages, or different CO_2 abundances/boundary conditions. Further inter-model comparison will be needed in order to clarify these discrepancies (Cooke et al. 2022).

Overall our results for O_3 formation are consistent with previous 1D studies and roughly similar to time-averaged results from 3D models. Despite this, it is important to remember that the night-sides of slowly rotating and tidally locked planets may have significantly more O_3 than the day-side, introducing phase-angle dependency on the amount of detectable O_3 for observations.

5.2. Factors that impact the O_2–O_3 relationship

The O_2–O_3 relationship is strongly dependent on the host star as well as the planetary atmospheric composition. Here we will briefly describe several ways the O_2–O_3 relationship can diverge from the results in this study.

We have shown that the O_2–O_3 relationship is highly influenced by the UV spectrum of the host star, both in terms of the

total amount of UV flux and the FUV/NUV flux ratio, with FUV primarily responsible for creating O_3, and NUV destroying it. In this study we selected stellar hosts from a range of spectral types, but have not yet explored the variation of UV activity and FUV/NUV ratios within specific spectral types. This is of particular importance for K and M dwarfs, as they are subject to larger amounts of UV variability, and thus greater variations in the O_2–O_3 relationship for the planets such stars host (e.g., France et al. 2013, 2016; Youngblood et al. 2016; Loyd et al. 2018). For instance, the UV spectrum for our M5V host star comes from GJ 876 which displays low amounts of chromospheric activity (France et al. 2016). If the stellar host in question was a more active star of a similar type, such as Proxima Centauri (classified as an M5.5V star; Boyajian et al. 2012; Anglada-Escudé et al. 2016), an orbiting Earth-like planet would be subject to a different O_2–O_3 relationship due to the significant change UV spectral slope of the star. A more in-depth study of the impact of varying UV activity levels for K and M dwarf planetary hosts will be necessary to fully understand how O_3 production would vary for different O_2 atmospheric abundances.

Another important aspect of this study to note is that the initial conditions of atmospheric species are kept constant across all models to better understand how the O_2–O_3 relationship differs for different host star spectra. However, the O_2–O_3 relationship could be altered by a variety of scenarios due to the potentially huge diversity of terrestrial planet atmospheric compositions.

The HO_x and NO_x catalytic cycles are the most prominent sinks for O_3 on modern Earth, and could significantly impact O_3 formation if there was an increase or decrease of the species powering these cycles. Therefore, changes in the amount of stratospheric H_2O or N_2O would alter the efficiency of O_3 destruction, as they are the primary sources of stratospheric HO_x and NO_x. On modern Earth H_2O is generally prevented from traveling into the stratosphere by the cold trap, although it can be created in the stratosphere via CH_4 reactions with OH (Reaction (23)), implying a change in CH_4 will additionally impact O_3 destruction. The impacts on the O_2–O_3 relationship as these abundances change will be explored at length in the next paper of this series. Reducing gases in general (e.g., CH_4, H_2) can impact O_2 and O_3 levels, whether produced biologically or through volcanic outgassing (e.g., Hu et al. 2012; Black et al. 2014; Gregory et al. 2021; Cooke et al. 2022). O_3 can also be depleted by cometary impacts (e.g., Marchi et al. 2021) and through solar flares (e.g., Pettit et al. 2018). In addition, O_3 can vary throughout different seasons on modern Earth (Olson et al. 2018).

Oxygen-bearing species in general can also influence the O_2–O_3 relationship, especially in situations where O_2 is produced abiotically via photolysis-driven production (see Meadows 2017 for full review). In particular, CO_2-rich atmospheres may create significant amounts of O_3 through CO_2 photolysis (Hu et al. 2012; Domagal-Goldman et al. 2014; Tian et al. 2014; Harman et al. 2015; Gao et al. 2015) around host stars with high FUV/NUV flux ratios. FUV photons ($\lambda < 200$ nm) photolyze CO_2,

$$CO_2 + h\nu \rightarrow CO + O, \tag{31}$$

to produce an O atom (or the $O(^1D)$ radical if $\lambda < 167$ nm; Reaction (21)). Oxygen atoms can combine to create O_2,

$$O + O + M \rightarrow O_2 + M, \tag{32}$$

which can then combine with O atoms to create O_3 (Reaction (2)). Because O_2 is photolyzed at shorter wavelengths than O_3 ($\lambda < 240$ nm, see Fig. 1), stellar hosts with high incident FUV/NUV flux ratios can allow abiotic O_3 accumulation without significant corresponding O_2 buildup (Hu et al. 2012; Domagal-Goldman et al. 2014; Tian et al. 2014; Harman et al. 2015). In such scenarios the O_3/O_2 ratio would be higher than what would be predicted if O_3 were formed directly from O_2, implying that a high O_3/O_2 ratio could indicate non-biological O_3 (and O_2) creation (Domagal-Goldman et al. 2014). However, it remains uncertain which types of stellar hosts would be favorable for this scenario. Some studies find Sun-like stars can accumulate significant O_3 through CO_2 photolysis if outgassing rates of reduced species are low (Hu et al. 2012), while others restrict this scenario to K and M dwarfs with high FUV/NUV flux ratios (Tian et al. 2014; Harman et al. 2015). This scenario might likewise be produced by F star hosts with their strong FUV fluxes, although with enough NUV flux, O_3 destruction rates could prevent O_3 buildup (Domagal-Goldman et al. 2014). Differences in model lower boundary conditions, which control the impact of different O_2 ground sinks, are likely to blame for the disparity in the capacity of O_3 to accumulate between different studies (Domagal-Goldman et al. 2014; Tian et al. 2014; Harman et al. 2015; Meadows 2017). Despite uncertainties in O_2 surface sinks, it is clear K/M dwarfs with high FUV/NUV ratios are susceptible, and potentially hotter stars with low abundances of reduced gaseous species. The effect of a CO_2-rich atmosphere on the O_2–O_3 relationship will be highly influenced by the host star and atmospheric abundances of reduced gaseous species.

Another method of creating O_3 without using the Chapman mechanism is via the "smog mechanism", which can produce O_3 photochemically using a volatile organic compound (i.e., CH_4) and NO_x. This process is responsible for smog pollution often occurring in large cities on modern Earth, but could also have occurred during the Proterozoic (2.5 Ga – 541 Ma) with high levels of CH_4 and NO_x (Grenfell et al. 2006). Under some circumstances Grenfell et al. (2006) computed that nearly double the amount of O_3 on modern Earth could have been produced with just 1% PAL O_2 via the smog mechanism. Additionally, Grenfell et al. (2013) found that the O_3 smog mechanism may become more efficient than the Chapman mechanism for habitable zone planets around late M dwarf with low UV that is less efficient at O_2 photolysis. Not only would O_3 created primarily by the smog mechanism rather than the Chapman mechanism change the O_2–O_3 relationship, but "smog" O_3 can be harmful for life. Smog mechanism O_3 is created in the troposphere rather than the stratosphere, and could result in significant ground-level O_3. Although on Earth our stratospheric O_3 protects life by shielding harmful UV, ground level O_3 on a smog-dominated planet can become fatal to Earth organisms at ~1 ppm.

Overall the O_2–O_3 relationship could be subject to large variations based both on the UV spectral slope of the host star, as well as atmospheric composition. Ozone formation via either CO_2 photolysis or hydrocarbon reactions would not be expected to resemble the O_2–O_3 relationship that "Earth-like" atmospheres would demonstrate. However, the FUV/NUV flux ratio of the host star may allow us to rule out certain certain scenarios without observations of the planetary atmosphere.

5.3. Can we infer O_2 abundance from an O_3 measurement?

Returning to the question that prompted this study: is O_3 a reliable proxy for O_2? Variations in the O_2–O_3 relationship (Sect. 5.2) would increase the difficulty in using O_3 to infer O_2 abundance, and would require additional atmospheric information to provide the proper context. For the sake of simplicity,

we will discuss the possibility of inferring O_2 from an O_3 measurement from our "Earth-like" models in this paper. But even in this simplified case where we keep initial conditions of all atmospheric species constant (apart from O_2 and O_3 and let them adapt to different stellar hosts) precisely determining O_2 from O_3 is not straightforward due to the nonlinear O_2–O_3 relationship.

Figure 3 clearly demonstrates that not only does the amount of O_3 created for different O_2 levels change significantly for different spectral types, but also the trend that the O_2–O_3 relationship will follow as O_2 is changed will depend on the stellar host. Section 4.1 details how planets around hotter stars with higher UV flux (G0V, Sun, K2V) all experience their maximum O_3 formation efficiency at O_2 levels lower that 100% PAL, while there is a continuous (albeit nonlinear) decrease of O_3 production for cooler hosts with lower UV flux (K5V, M5V). Whether a model atmosphere experiences an increase in O_3 production as O_2 decreases (as seen for hotter stars) is dependent primarily on whether O_2 photolysis ($\lambda < 240$ nm) can reach deep into the atmosphere. The total amount of O_3 depends on the FUV/NUV flux ratio of the host star as well, with FUV flux creating O_3 while NUV wavelengths will cause its destruction (see Sects. 3.2 and 4.1). Although the K2V-hosted models demonstrate this effect with the maximum amount of O_3 production occurring at 55% PAL O_2, for models at O_2 levels near 100% PAL O_2 the K5V and M5V hosts have higher O_3 abundances due to their larger FUV/NUV ratios. Therefore, to predict the O_2–O_3 relationship for a given star even with knowledge of "Earth-like" conditions knowing both the total UV emitted and UV spectral slope of the host star will be essential.

Idealized planetary emission spectra of the 9.7 μm O_3 features in Fig. 7 show a non-trivial relationship between both O_2 and O_3 abundance and spectral feature depth for hotter stellar hosts, with more "straightforward" correlation of O_2 and O_3 abundances and feature depth for cooler hosts (K5V, M5V). This is due to the dependence of feature strength in emission spectra on the atmospheric temperature profile, with O_3 measurements being particularly complicated by the fact that O_3 highly influences stratospheric heating. Measuring O_3 abundance from an emission spectra will require modeling of atmospheric temperature and pressure profiles for an accurate estimate, especially for stars emitting enough UV capable of creating and absorbing O_3 for significant stratospheric heating. Smaller amounts of O_3 as created by cooler stars have less of an impact on stratospheric heating, and therefore will maintain a more consistent temperature profile even for large variation in O_2 abundance.

Even operating under the unlikely assumption that an accurate measurement of atmospheric O_3 could be done, inferring O_2 abundance will still not be straightforward, especially for hotter host stars (G0V, Sun, K2V) where O_3 does not always decrease as O_2 levels decrease. For example, in our Sun-hosted models the total integrated O_3 column density at 150% PAL O_2 is roughly the same as the amount at 5% PAL O_2 (4.92×10^{18} cm^{-2} and 4.80×10^{18} cm^{-2}, respectively). This implies that for hotter stellar hosts, it is unlikely O_2 could be well constrained from an O_3 measurement for relatively high levels of O_2. It could, however, be possible to use an O_3 measurement to differentiate between pre- and post-GOE O_2 levels, as well as infer the existence of a substantial O_3 layer providing surface UV shielding. Due to the consistent decrease in O_3 abundance with decreasing O_2 for cooler hosts, it appears that inferring O_2 from O_3 may be much simpler for planets orbiting cooler stars that those around hotter stars. It is important to note that specific knowledge of the UV spectral slope for cool K and M dwarfs will be extremely important to model O_3 levels, especially due to the increased likelihood of O_3 buildup via abiotic means and the diversity of activity levels (hence FUV/NUV flux ratios) around such stars.

5.4. Is it necessary to constrain O_2 abundance for O_3 to be a useful biosignature?

Although inferring O_2 levels precisely from O_3 measurements will not be possible for hot stellar hosts and will still require additional atmospheric context and knowledge of the UV spectral slope for cooler hosts, what does this mean for O_3 as a biosignature? Would it be necessary to infer O_2 for O_3 to be a useful indicator of life, or could it serve as a promising biosignature without precise O_2 information? Two of the strongest arguments against O_2 as a biosignature are 1) it can be produced abiotically, and 2) it has been at relatively high abundances for only a small fraction of Earth's geological history (see review in Meadows 2017; Meadows et al. 2018b). We examine these arguments as they pertain to O_3 as a biosignature.

The multiple proposed pathways for abiotic O_2 production will prevent O_3 from being a "standalone" biosignature as well. These mechanisms include production via CO_2 photolysis as discussed in Sect. 5.3, as well as via H_2O photolysis either from an extremely active pre-main sequence star (Luger & Barnes 2015; Tian 2015) or an atmosphere that has allowed H_2O to enter the stratosphere due to a lack of cold trap from low abundances of non-condensable gases (Wordsworth & Pierrehumbert 2014). Ruling out these scenarios could be possible by detections or non-detections of gaseous species that would be produced or destroyed during these processes. For example, O_2 and O_3 abiotic buildup from CO_2 photolysis could be revealed via a detection of CO, sometimes called an "antibiosignature" (for detailed descriptions of these mechanisms and their spectral discriminants see Meadows 2017; Meadows et al. 2018b).

Potential abiotic production will require contextual knowledge of an atmosphere to use either O_2 or O_3 as a biosignature. Abiotic buildup from CO_2 photolysis with high FUV/NUV flux ratio stellar hosts could potentially impact O_3 more than O_2, as it is possible to accumulate O_3 more easily than O_2 in this scenario, and could potentially allow simultaneous detection of abiotic O_3 and CH_4 under certain conditions (Domagal-Goldman et al. 2014). However, predictions of abiotic O_2 and O_3 buildup are dependent on the lower boundary conditions of the model in question, so these estimates vary (Hu et al. 2012; Domagal-Goldman et al. 2014; Tian et al. 2014; Harman et al. 2015; Gao et al. 2015). Detections or non-detections of CO and CO_2 will be important especially in assessing the origin of an O_3 detection.

The second main argument against O_2 as a reliable biosignature (even when accounting for abiotic sources) is that O_2 levels have only been relatively high for a short period of Earth's geological history. Oxygenic photosynthesis is thought to have been first used by cyanobacteria ~2.7 Ga, although O_2 buildup during the GOE was not thought to have occurred until ~2.5 Ga (e.g., Poulton et al. 2020). O_2 levels comparable to modern Earth were not reached until the Phanerozoic (541 Ma – present day) sparked by the Cambrian explosion when land began to be colonized by plants (Lenton & Daines 2017; Dahl & Arens 2020). Before the GOE O_2 levels were expected to be well below $10^{-}3$% PAL, and potentially remained relatively low during the majority of the Proterozoic (2.5 Ga–541 Ma) with estimates ranging from ~0.3–10% PAL O_2 (e.g., Catling et al. 2018). Even if the lowest O_2 estimates for the Proterozoic were reality (~0.01% PAL O_2), there is evidence of an O_3 layer after 2.4 Ga (Crockford et al. 2018). Although an O_2 detection would be extremely difficult at this abundance, it has been suggested that O_3 could reveal this

undetectable O_2 (e.g., Leger et al. 1993; Des Marais et al. 2002; Segura et al. 2003; Léger et al. 2011; Harman et al. 2015). Results of this paper only further prove this point, especially around hotter stars (see Fig. 3). For the G0V and Sun-hosted planets even at a level of 0.01% PAL O_2, they still produce ~15% the amount of O_3 they do at 100% PAL O_2. This number falls to ~2% for the M5V-hosted planet, although it still demonstrates a less drastic decrease in O_3 as O_2 decreases. This implies that especially for planets orbiting hotter stars that O_3 is a much longer lived detectable biosignature than O_2 for an Earth-like planet, as detections may be sensitive to Proterozoic O_3 levels.

Although gaining precise information about O_2 abundance from an O_3 measurement will be extremely difficult or not possible (see discussion in Sect. 5.3), knowing O_3 abundance alone would still provide valuable information about the atmosphere. There appears to be a "bistability limit" for atmospheric O_2, implying that certain O_2 levels would not be stable in the atmosphere due to O_2 sinks and geochemical cycles, as atmosphere switches from reduced to oxidizing (e.g., Segura et al. 2003; Goldblatt et al. 2006). Gregory et al. (2021) calculated that there are only a few stable solutions with O_2 abundances between 3×10^{-6} and 1% PAL for an Earth-like planet orbiting the Sun. The existence of this "bistability limit" could explain the ~300 Myr delay between the advent of oxygenic photosynthesis and appreciable O_2 accumulation in the atmosphere (Goldblatt et al. 2006). O_3 abundance drastically falls off for all our host stars under 0.01% PAL O_2, implying that an O_3 detection would allow us to distinguish between pre- and post-GOE O_2 levels with relative ease. In the search for Earth-like planets, O_3 appears to be a viable biosignature for a much longer portion of Earth's history, potentially allowing us to infer the existence of oxygenic photosynthesis for much longer than an O_2 detection.

Although O_3 is not created by life, its UV shielding capabilities could allow estimates of whether the surface environment is safe for life. As seen in Fig. 6 and Table 4, the amount of UV flux reaching the planetary surface begins to converge quickly to the UV incident upon the planet when O_2 abundance drops below 1% PAL, and it has been predicted that O_2 levels less than this will not be efficient at preventing DNA damage (e.g., Segura et al. 2003). If an upper O_2 "bistability limit" indeed exists at 1% PAL (Gregory et al. 2021), a detection of O_3 in a planetary atmosphere could imply a certain amount of UV shielding, and potential surface life.

However, it is important to remember that the first evidence of life dates back 3.7 Ga, long before the GOE, or even oxygenic photosynthesis (Rosing 1999). Although O_3 may be a longer lived biosignature than O_2 and can indicate substantial UV surface shielding, a non-detection of O_3 (or O_2) could not rule out the existence of life. Although the surface UV environment would have been harsh before the GOE, it is possible that without a UV screen that life could thrive in the photic zone of the ocean, and perhaps colonize land (Cockell & Raven 2007). It has even been suggested that a significant amount of UV may have been necessary to synthesize prebiotic molecules (e.g., Patel et al. 2015; Ranjan & Sasselov 2016; Rimmer et al. 2018). Even substituting O_3 for O_2 in biosignature searches, life on pre-GOE Earth would be undetectable.

6. Conclusions

In this first part of our paper series we show that the nonlinear O_2–O_3 relationship varies significantly for model atmospheres of planets orbiting different types of host stars, with different trends for planets with hotter host stars versus those with cooler host stars. As seen in Fig. 3, planets orbiting hotter host stars display peak O_3 abundance at lower O_2 levels than modern Earth, while planets with cooler hosts have O_3 decrease along with O_2. The increase in O_3 at lower O_2 levels for hotter host stars is due to the O_3 layer shifting downward in the atmosphere as O_2 levels (and its ability to absorb UV) decrease. At these deeper and denser levels of the atmosphere the 3-body reaction that creates O_3 (Reaction (2)) allows more efficient O_3 production than at high O_2 abundances. Cooler stars do not experience this effect since it requires a stronger incident FUV flux to push O_3 formation deep enough in the atmosphere to allow for much faster production.

As O_2 decreases in the atmosphere, photolysis of many gaseous species as well as $O(^1D)$ production will occur at lower atmospheric levels. The biologically relevant molecules H_2O, CH_4, and N_2O all experience upper atmospheric depletion to different degrees, with these effects significantly more prominent around host stars with higher UV fluxes (Fig. 4). As O_2 decreases and photolysis rates increase, HO_x species are primarily pushed to lower altitudes rather than destroyed, while NO_x species are destroyed by photolysis as well as produced at lower atmospheric levels (Fig. 5).

UVA and UVB wavelengths are only partially shielded by O_3, so the amount of photons in this wavelength range that reach the planetary surface scales with the amount of incident UVA and UVB flux. However, for biologically damaging UVC photons, there is a much stronger dependence on both O_2 and O_3 abundance. For high O_2 levels, our hottest host star (G0V) had the lowest surface UVC flux, despite also having the highest incident UVC flux (Fig. 6). As O_2 and O_3 abundances decreases these UVC surface levels begin to converge to incident UVC flux as UV shielding becomes inefficient.

Ozone features in planetary emission spectra were found to require knowledge of the atmospheric temperature profiles, as the depth of features is dictated by the temperature difference between the emitting and absorbing layers of the gaseous species. Since O_3 NUV absorption is a significant source of stratospheric heating, a large amount of O_3 along with significant incident NUV flux will cause a smaller temperature difference between the stratosphere and planetary surface, resulting in a shallower spectral feature (Fig. 7). For cooler stars with slower O_3 production, and therefore less stratospheric temperature inversion, O_2 spectral features are more intuitive to interpret. Overall it is clear that interpreting any observation of O_3 will require the UV spectrum of the host star as well as photochemical and climate modeling of the planetary atmosphere.

Now that we have explored the O_2–O_3 relationship and its impact on planetary emission spectra, let us now return again to our original question: is O_3 a reliable proxy for O_2? In short, the complicated nature of the O_2–O_3 relationship tells us that O_3 is not a reliable tracer of O_2. Our results show us that for hotter stars, using O_3 as a precise tracer for O_2 will not be possible due to the degeneracies in the O_2–O_3 relationship, and for cooler stars it will be very difficult without knowledge of the UV spectrum of the host star as well as planetary atmospheric composition. However, an O_3 measurement on its own is still an insightful measurement, even if it does not provide precise information on O_2 abundance. Not only is O_3 detectable in trace amounts (unlike O_2), it additionally allows for an assessment of the UV surface environment of the planet.

There is likely no "standalone" atmospheric biosignature, but either O_2 or O_3 along with atmospheric context could provide evidence of oxygenic photosynthesis. Both will require detections of other gaseous species to rule out various mechanisms for

abiotic O_2 or O_3 production. Although it is important to note that a CO_2 rich planet may be more likely to have an abiotic buildup of O_3 without O_2 – a strike against O_3 as a biosignature gas (see Sect. 5.2 for detailed discussion). However, there is a strike against O_2 in comparison to O_3:O_2 has only existed on Earth in relatively high amounts for a short fraction of Earth's geological history. Ozone, on the other hand, is detectable in trace amounts, potentially making it a longer lived detectable biosignature for Earth-like planets. It seems that neither O_2 or O_3 is inherently a "better" biosignature than the other; simply that they give different information and can be more or less useful depending on the scenario. With knowledge of the UV spectrum of the host star along with careful climate and photochemistry modeling we can begin to understand the O_2–O_3 relationship and use O_3 as a reliable indicator for oxygenic photosynthesis.

Acknowledgements. We thank both the anonymous referee and journal editor for their comments which helped improve the clarity of this manuscript. All computing was performed on the HPC cluster at the Technical University of Denmark (DTU Computing Center 2021). This project is funded by VILLUM FONDEN.

References

Anglada-Escudé, G., Amado, P. J., Barnes, J., et al. 2016, Nature, 536, 437
Arney, G., Domagal-Goldman, S. D., Meadows, V. S., et al. 2016, Astrobiology, 16, 873
Arney, G. N., Meadows, V. S., Domagal-Goldman, S. D., et al. 2017, ApJ, 836, 49
Batalha, N. E., Marley, M. S., Lewis, N. K., & Fortney, J. J. 2019, ApJ, 878, 70
Batalha, N., Rooney, C., & MacDonald, R. 2021, https://doi.org/10.5281/zenodo.5093710
Bétrémieux, Y., & Kaltenegger, L. 2013, ApJ, 772, L31
Bétrémieux, Y., & Kaltenegger, L. 2014, ApJ, 791, 7
Black, B. A., Lamarque, J.-F., Shields, C. A., Elkins-Tanton, L. T., & Kiehl, J. T. 2014, Geology, 42, 67
Boyajian, T. S., von Braun, K., van Belle, G., et al. 2012, ApJ, 757, 112
Brasseur, G. P., & Solomon, S. 2005, Aeronomy of the Middle Atmosphere: Chemistry and Physics of the Stratosphere and Mesosphere (Dordrecht: Springer), 221
Carone, L., Keppens, R., Decin, L., & Henning, T. 2018, MNRAS, 473, 4672
Catling, D. C., & Kasting, J. F. 2017, Atmospheric Evolution on Inhabited and Lifeless Worlds (Cambridge, UK: Cambridge University Press)
Catling, D. C., Krissansen-Totton, J., Kiang, N. Y., et al. 2018, Astrobiology, 18, 709
Chapman, S. A. 1930, Mem. R. Met. Soc., 3, 103
Chen, H., Wolf, E. T., Kopparapu, R., Domagal-Goldman, S., & Horton, D. E. 2018, ApJ, 868, L6
Cockell, C. S., & Raven, J. A. 2007, Phil. Trans. R. Soc. A., 365, 1889
Cooke, G. J., Marsh, D. R., Walsh, C., Black, B., & Lamarque, J. F. 2022, Roy. Soc. Open Sci., 9, 211165
Crockford, P. W., Hayles, J. A., Bao, H., et al. 2018, Nature, 559, 613
Crutzen, P. J., & Lelieveld, J. 2001, Annu. Rev. Earth Planet. Sci., 29, 17
Dahl, T. W., & Arens, S. K. 2020, Chem. Geol., 547, 119665
Des Marais, D. J., Harwit, M. O., Jucks, K. W., et al. 2002, Astrobiology, 2, 153
Domagal-Goldman, S. D., Segura, A., Claire, M. W., Robinson, T. D., & Meadows, V. S. 2014, ApJ, 792, 90
DTU Computing Center 2021, DTU Computing Center resources
Fauchez, T. J., Villanueva, G. L., Schwieterman, E. W., et al. 2020, Nat. Astron., 4, 372
France, K., Froning, C. S., Linsky, J. L., et al. 2013, ApJ, 763, 149
France, K., Loyd, R. O. P., Youngblood, A., et al. 2016, ApJ, 820, 89
Gao, P., Hu, R., Robinson, T. D., Li, C., & Yung, Y. L. 2015, ApJ, 806, 249
Goldblatt, C., Lenton, T. M., & Watson, A. J. 2006, Nature, 443, 683
Gregory, B. S., Claire, M. W., & Rugheimer, S. 2021, Earth Planet. Sci. Lett., 561, 116818
Grenfell, J. L., Stracke, B., Patzer, B., Titz, R., & Rauer, H. 2006, Int. J. Astrobiol., 5, 295
Grenfell, J. L., Stracke, B., von Paris, P., et al. 2007, Planet. Space Sci., 55, 661
Grenfell, J. L., Gebauer, S., Godolt, M., et al. 2013, Astrobiology, 13, 415
Grenfell, J. L., Gebauer, S., v. Paris, P., Godolt, M., & Rauer, H. 2014, Planet. Space Sci., 98, 66
Harman, C. E., Schwieterman, E. W., Schottelkotte, J. C., & Kasting, J. F. 2015, ApJ, 812, 137
Hu, R., Seager, S., & Bains, W. 2012, ApJ, 761, 166
Kaltenegger, L., MacDonald, R. J., Kozakis, T., et al. 2020, ApJ, 901, L1
Kasting, J. F. 1979, PhD thesis, University of Michigan, USA
Kasting, J. F., & Ackerman, T. P. 1986, Science, 234, 1383
Kasting, J. F., & Donahue, T. M. 1980, J. Geophys. Res., 85, 3255
Kasting, J. F., Holland, H. D., & Pinto, J. P. 1985, J. Geophys. Res. 90, 10497
Kiesecker, J. M., Blaustein, A. R., & Belden, L. K. 2001, Nature, 410, 681
Kitzmann, D., Patzer, A. B. C., von Paris, P., Godolt, M., & Rauer, H. 2011, A&A, 531, A62
Kopparapu, R. K., Ramirez, R., Kasting, J. F., et al. 2013, ApJ, 770, 82
Kozakis, T., & Kaltenegger, L. 2019, ApJ, 875, 99
Kozakis, T., Kaltenegger, L., & Hoard, D. W. 2018, ApJ, 862, 69
Kump, L. 2008, Nature, 451, 277
Kurucz, R. L. 1979, ApJS, 40, 1
Lederberg, J. 1965, Nature, 207, 9
Leger, A., Pirre, M., & Marceau, F. J. 1993, A&A, 277, 309
Léger, A., Fontecave, M., Labeyrie, A., et al. 2011, Astrobiology, 11, 335
Lenton, T. M. & Daines, S. J. 2017, Annu. Rev. Mar. Sci., 9, 31
Levine, J. S., Hays, P. B., & Walker, J. C. G. 1979, Icarus, 39, 295
Lin, Z., MacDonald, R. J., Kaltenegger, L., & Wilson, D. J. 2021, MNRAS, 505, 3562
Lincowski, A. P., Meadows, V. S., Crisp, D., et al. 2018, ApJ, 867, 76
Lippincott, E. R., Eck, R. V., Dayhoff, M. O., & Sagan, C. 1967, ApJ, 147, 753
Lovelock, J. E. 1965, Nature, 207, 568
Loyd, R. O. P., France, K., Youngblood, A., et al. 2018, ApJ, 867, 71
Luger, R., & Barnes, R. 2015, Astrobiology, 15, 119
Madden, J., & Kaltenegger, L. 2020, MNRAS, 495, 1
Marchi, S., Drabon, N., Schulz, T., et al. 2021, Nat. Geosci., 14, 827
Meadows, V. S. 2017, Astrobiology, 17, 1022
Meadows, V. S., Arney, G. N., Schwieterman, E. W., et al. 2018a, Astrobiology, 18, 133
Meadows, V. S., Reinhard, C. T., Arney, G. N., et al. 2018b, Astrobiology, 18, 630
Misra, A., Meadows, V., & Crisp, D. 2014, ApJ, 792, 61
Olson, S. L., Schwieterman, E. W., Reinhard, C. T., et al. 2018, ApJ, 858, L14
Patel, B., Percivalle, C., Ritson, D., Duffy, D., & Sutherland, J. 2015, Nat. Chem., 7, 301
Pettit, J., Randall, C. E., Marsh, D. R., et al. 2018, J. Geophys. Res. (Space Phys.), 123, 5747
Poulton, S. W., Bekker, A., Cumming, V., et al. 2020, Nature, 592, 232
Proedrou, E., & Hocke, K. 2016, Earth Planets Space, 68, 96
Quanz, S. P., Absil, O., Benz, W., et al. 2021, Exp. Astron. [arXiv:1908.01316]
Ranjan, S., & Sasselov, D. D. 2016, Astrobiology, 16, 68
Ranjan, S., Schwieterman, E. W., Harman, C., et al. 2020, ApJ, 896, 148
Ratner, M. I., & Walker, J. C. G. 1972, J. Atmos. Sci., 29, 803
Rimmer, P. B., Xu, J., Thompson, S. J., et al. 2018, Sci. Adv., 4, eaar3302
Rosing, M. T. 1999, Science, 283, 674
Rugheimer, S., Kaltenegger, L., Zsom, A., Segura, A., & Sasselov, D. 2013, Astrobiology, 13, 251
Rugheimer, S., Kaltenegger, L., Segura, A., Linsky, J., & Mohanty, S. 2015a, ApJ, 809, 57
Rugheimer, S., Segura, A., Kaltenegger, L., & Sasselov, D. 2015b, ApJ, 806, 137
Schwieterman, E. W., Kiang, N. Y., Parenteau, M. N., et al. 2018, Astrobiology, 18, 663
Segura, A., Krelove, K., Kasting, J. F., et al. 2003, Astrobiology, 3, 689
Segura, A., Kasting, J. F., Meadows, V., et al. 2005, Astrobiology, 5, 706
Segura, A., Walkowicz, L. M., Meadows, V., Kasting, J., & Hawley, S. 2010, Astrobiology, 10, 751
Selsis, F., Despois, D., & Parisot, J. P. 2002, A&A, 388, 985
Teal, D. J., Kempton, E. M. R., Bastelberger, S., Youngblood, A., & Arney, G. 2022, ApJ, 927, 90
Tian, F. 2015, Earth Planet. Sci. Lett., 432, 126
Tian, F., France, K., Linsky, J. L., Mauas, P. J. D., & Vieytes, M. C. 2014, Earth Planet. Sci. Lett., 385, 22
Toon, O. B., McKay, C. P., Ackerman, T. P., & Santhanam, K. 1989, J. Geophys. Res., 94, 16287
Wordsworth, R., & Pierrehumbert, R. 2014, ApJ, 785, L20
Wunderlich, F., Godolt, M., Grenfell, J. L., et al. 2019, A&A, 624, A49
Yates, J. S., Palmer, P. I., Manners, J., et al. 2020, MNRAS, 492, 1691
Youngblood, A., France, K., Loyd, R. O. P., et al. 2016, ApJ, 824, 101
Zahnle, K., Claire, M. W., & Catling, D. 2006, Geobiology, 4, 271